Impact of wave-dependent stress on storm surge simulations in the North Sea: Ocean model evaluation against in situ and satellite observations

Lucia Pineau-Guillou, Marie-Noëlle Bouin, Fabrice Ardhuin, Florent Lyard, Jean-Raymond Bidlot, Bertrand Chapron

Impact of wave-dependent stress on storm surge simulations in the North Sea: ocean model evaluation against in situ and satellite observations

Lucia Pineau-Guillou[a,*], Marie-Noëlle Bouin[a,b], Fabrice Ardhuin[a], Florent Lyard[c], Jean-Raymond Bidlot[d], Bertrand Chapron[a]

[a] *IFREMER, CNRS, IRD, UBO, Laboratoire d'Océanographie Physique et Spatiale, UMR 6523, IUEM, Brest, France*
[b] *CNRM, UMR 3589, Météo-France et CNRS, Toulouse, France*
[c] *Laboratoire d'Etudes en Géophysique et Océanographie Spatiales, Centre National de la Recherche Scientifique, Toulouse, France*
[d] *European Centre for Medium-range Weather Forecasts, Reading, UK*

Abstract

We investigate the impact of wave-dependent stress on surge modelling, from case studies in the North Sea, using a global ocean model forced with a wave-atmosphere coupled model. We select the storms with the largest surges and a range of sea state development from young to mature seas. The modelled surges are compared to tide gauges and altimeter data. The ocean model is able to accurately predict storm surges in coastal areas. The consistency of the model outputs, the altimeter, and the tide gauge data confirms the accuracy of altimeters for storm surge measurements. We show that using a wave-dependent rather than a wind-dependent only stress formulation gives more accurate surge simulations when the sea state is young and the sea rougher. Taking into account the waves in the stress formulation has a significant impact on the surges (up to 20 cm).

Keywords: air-sea exchanges, storm surges, wind stress, drag coefficient, wind-wave coupling, North Sea

1. Introduction

Storm surges are generated by atmospheric pressure gradient and wind stress. In coastal areas, the wind stress contribution is more effective due to shallow waters, water pileup along the coast, and resonant effects (Moon et al., 2009; Bertin et al., 2012). In addition, in nearshore areas, the radiation stress, which is the momentum flux carried by the waves, generates nearshore currents and wave setup (i.e. additional surge) when the waves dissipate (Bunya et al., 2010; Kim et al., 2010; Brown et al., 2010; Idier et al., 2012; Lee et al., 2013; Bertin et al., 2015; Thuy et al., 2017; Choi et al., 2018). Here, we focus on the impact of the wind stress on the surges. This study tackles the question 'which impact has the sea state on the wind stress?'. To answer this, we determine if simulated surges are closer to observations when wind stress parameterization is wave-dependent.

The wind stress is usually parameterized using bulk formulae that express it as a function of the wind speed at a given height, generally 10 m above sea surface, and of a drag coefficient

$$\tau = \rho_a u_*^2 = \rho_a C_d U_{10}^2 \qquad (1)$$

where u_*, C_d, and U_{10} are the friction velocity, the drag coefficient, and the wind speed at 10 m above the surface, respectively. Most formulations of the drag depend only on the wind speed (e.g. Moon et al., 2007; Edson et al., 2013; Peng and Li, 2015), whereas others include sea state

*Corresponding author
Email address: lucia.pineau.guillou@ifremer.fr (Lucia Pineau-Guillou)

parameters (e.g. Janssen, 1991; Moon et al., 2009). Despite years of research, the impact of sea state on drag remains inconclusive. Recently, Edson et al. (2013) concluded that the "COARE 3.5 wind speed-dependent formulation matches the observations well without any wave information," whereas earlier works insisted on the importance of wave-enhanced drag for young waves (Mastenbroek et al., 1993).

These contrasted results can be explained by the complexity of the problem. There are major issues that prevent a simple answer to the question 'what is the wave impact on the wind stress, if any?': (1) Wind stress measurements - and drag estimations - are difficult to perform, particularly at high winds. Uncertainties in observations could explain the variability of the drag at a given wind speed. Estimations from several recent field experiments based on direct in situ measurements (e.g. Black et al., 2007; Edson et al., 2013) or indirect ones (Powell et al., 2003; Jarosz et al., 2007; Holthuijsen et al., 2012), as well as laboratory tank measurements (e.g. Donelan et al., 2004; Takagaki et al., 2012) show differences in the drag up to a factor 2 at 30 m/s (Pineau-Guillou et al., 2018). It is not known if these differences are due to measurement uncertainties or various environmental conditions (fetch, turning wind, bathymetry...). (2) Wind stress measurements are scarce. They generally come from short dedicated campaigns, with moderate winds often being lower than 20 m/s. There is clearly a lack of measurements at very high winds. (3) All the variables used to explain the drag variability are interdependent. Consequently, good correlations between the drag and variables such as wave age may mainly be due to self-correlation (Andreas, 2009). This contributes to a lack of confidence in these relationships in a part of the scientific community.

The objective of this article is to investigate the impact of a wave-dependent stress on the surges. Here, we focus on the North Sea. The main idea is to simulate storms with various sea states (i.e. young and old) to estimate the sensitivity of surges to the sea state development (i.e. the wave age). Selected storms are simulated using wind-dependent only and wave-dependent stress parameterizations. The simulated surges are evaluated against observations (i.e. tide gauges and altimeters). The first part of the article describes the methods to compute the surges in models and observations. In the following part, we describe the case studies—namely, the storms selection, the numerical setup, and the validation data. Then, we analyze the results to estimate the impact of the wave-dependent stress on the storm surges. Finally, we discuss different points; among them is the difficulty of comparing the model with observations, as various processes contribute to the surges, particularly in coastal areas.

2. Surges in models and observations

The surges are the differences between the water level and the tide prediction. Here, we describe the methods to compute the surges from the model and observations.

2.1. Modelled surges

Surges are simulated with an ocean model forced with output from an atmosphere model. The ocean model resolves the classical Saint-Venant shallow water continuity and momentum equations in barotropic mode, formulated similarly as in Bertin et al. (2012)

$$\frac{\partial \eta}{\partial t} + \overrightarrow{\nabla}.\int_{-h}^{\eta} \vec{u} dz = 0, \quad (2)$$

$$\frac{D\vec{u}}{Dt} = -f\vec{k} \times \vec{u} + \alpha g \vec{\nabla}\hat{\psi} - \frac{\vec{\nabla}P_a}{\rho} - g\vec{\nabla}\eta + \frac{\overrightarrow{\tau_s} - \overrightarrow{\tau_b}}{\rho(\eta+h)} \quad (3)$$

where η is the surface elevation, $\vec{u}$ is the horizontal velocity, h is the bathymetry, f is the Coriolis parameter, α is the earth-elasticity factor, g is the mean gravitational acceleration, $\hat{\psi}$ is the earth tidal potential, P_a is the sea level atmospheric pressure, ρ is the water density, τ_s is the surface stress, and τ_b is the bottom stress. The bottom stress is expressed as

$$\overrightarrow{\tau_b} = \frac{C}{H} \parallel \vec{u} \parallel \vec{u} \quad (4)$$

where H is the mean local depth, and C is a dimensionless friction coefficient set as 2.5 10^{-3} (Lyard et al., 2006).

The water level variations are due to tide through the tidal potential ($\hat{\psi}$ in Eq. 3), wind through the wind stress (τ_s in Eq. 3), and atmospheric pressure through the pressure gradient ($\vec{\nabla} P_a$ in Eq. 3). Note that the wind stress effect is modulated with the bottom stress effect (τ_b in Eq. 3), whose influence is not studied here. We investigated the relative contribution of the wind stress and pressure gradient terms in Eq. 3 as $\overrightarrow{\tau_s}/\rho(\eta + h)$ and $\vec{\nabla} P_a/\rho$, respectively. In this case, the wind stress contribution increases in shallow waters, as it is divided by the water height. Comparison of the two terms shows that the wind stress term is largely dominant in the North Sea, that is, more than 90% of the sum of the two terms (Pineau-Guillou, 2018). This suggests that the currents are mainly driven by the wind, whereas the effect of the atmospheric pressure is negligible.

In the following, the surges are computed from simulations without tide (no tidal potential $\hat{\psi}$ in Eq. 3) and with atmospheric forcing only. As a consequence, the modelled surges correspond only to atmospheric surges; the surges due to wave breaking (i.e. wave setup) are not modelled here (see discussion in section 5). To compute the surges, we used the TUGO shallow water global ocean model, developed by LEGOS (Lyard et al., 2006). This model in barotropic mode resolves the classical shallow water continuity and momentum equations (Eqs 2 and 3). Following Lynch and Gray (1979), the model solves the generalized wave equation

$$\frac{\partial(CE)}{\partial t} + c_0 CE = 0 \quad (5)$$

where $CE = 0$ is the continuity equation (Eq. 2), and c_0 is a relaxation coefficient towards the continuity equation. This gives more explicitly

$$\frac{\partial^2 H}{\partial t^2} + \vec{\nabla}.\frac{\partial H\vec{u}}{\partial t} + c_0\left(\frac{\partial H}{\partial t} + \vec{\nabla}.H\vec{u}\right) = 0 \quad (6)$$

where $H = \eta + H$ is the water height, and $\frac{\partial H\vec{u}}{\partial t}$ is formally replaced by using the momentum equations. This allows to make the elevation solver implicit, hence relaxing the CFL condition for time step. Actually, TUGO can use different solvers and discretization for the dynamical equations, but the most efficient so far in tides or storm surges modelling is the LGP1xLGP1 (elevations and currents discretized at element vertices) generalized wave equations solver (hence being used in our study). TUGO is a reference model; it allowed the development of the tidal model FES2014 (Carrère et al., 2015), a worldwide reference model for tides, which is widely used in the scientific community. It also produces Dynamic Atmospheric Corrections to correct altimeter data from atmospheric effects (Carrère and Lyard, 2003). This correction is officially used by CNES and NASA for altimeter data processing.

147 *2.2. Observed surges*
148
149 Tide gauges measure the sea level. The surges are computed as the differences between the
150 observed and predicted sea level (Simon, 2007):
151
152 $$Surge_{TideGauge} = Observed\ sea\ level - Tide\ prediction \qquad (7)$$
153
154 We used 101 tide gauges in the North Sea (Figure 1), obtained thanks to Copernicus Marine
155 Environment Monitoring Service (CMEMS). Data temporal resolution is generally of 10
156 minutes (88% of the tide gauges) and sometimes 1 hour (12% of the tide gauges). We used the
157 Tidal ToolBox developed by LEGOS (Allain, 2013) to process the data and estimate the surges.
158 The method is the following; (1) a harmonic analysis is performed on the sea level observations
159 to estimate the harmonic constants (amplitude and phase) of the tidal constituents; (2) from
160 these harmonic constants, a prediction is computed over the same period as the observations;
161 (3) the surges are the differences between the observed and predicted sea levels (Eq. 7). Note
162 that this residual also includes the error associated with the prediction.
163
164 In addition to tide gauges, radar altimeters onboard satellites also measure the sea level—that
165 is, the instantaneous Sea Surface Height (SSH) above the ellipsoid. Data are processed by
166 providers to compute the Mean Sea Surface (MSS) and the Sea Level Anomaly (SLA). The
167 MSS corresponds to the mean of several years of SSH, eventually using several satellites. The
168 SLA is the difference between the instantaneous SSH and the MSS. Many geophysical and
169 environmental corrections are made to estimate SLA, and one among them is Dynamic
170 Atmospheric Correction (DAC) (Antony et al., 2014). This correction corresponds to the ocean
171 response to atmospheric forcing (atmospheric pressure and winds) and generally comes from
172 an ocean model elevations for high frequency part (e.g. TUGO, Carrère and Lyard (2003)) and
173 inverted barometer law for low-frequency part (e.g. using ECMWF atmospheric pressure
174 products). To be consistent with the model and the tide gauges, the surges from altimeters are
175 computed as the summation of the SLA and the DAC:
176
177 $$Surge_{Altimeter} = SLA + DAC. \qquad (8)$$
178
179 To compute the altimetric surges, we used the SLA and DAC from the JASON-2 1Hz X-
180 TRACK coastal product (Birol et al., 2016), developed by the Center of Topography of the
181 Ocean and Hydrosphere (CTOH/LEGOS, Toulouse). Along-track data have a temporal
182 resolution of 1 s, which corresponds to a spatial interval of about 6-7 km between points. X-
183 TRACK is a post-processing software which increases the SSH information derived from
184 satellite altimetry in the coastal ocean areas. Retrieved information along tracks come closer to
185 land, up to 5 km, against 10 km with the standard AVISO (Archiving, Validation and
186 Interpretation of Satellite Oceanographic data) product.
187
188 **3. Case studies and modelling**
189
190 Here, we describe the storms selection, the numerical setup, and the validation data.
191
192 *3.1. Storms selection*
193
194 The storms were selected according to the following criteria: 1) availability of good-quality
195 data at tide gauges as well as along tracks, 2) occurrence of maximum surges in the North Sea,
196 and 3) presence of various sea states. The objective was to select two storms with young sea

states, and two with old sea states. A common way to characterize the sea state is to consider the wave age, following the expression $\xi = C_p/U_{10}$, where C_p is the phase velocity at the peak of the wave spectrum, and U_{10} is the wind speed at 10 meters. When the wind has just started blowing, the waves are short-period, steep, and short-crested. At this stage, the wind speed is higher than the wave phase velocity, and the waves are growing. It is commonly considered that the value of 1.2 separates the young and the old sea. In the North Sea during the storms, the wave age is generally around 0.8 (Pineau-Guillou, 2018). In the following, sea state is considered as "young" when the wave age is close to 0.8 and "old" when the wave age is greater than 1.2 (swell). Note that the sea state quickly evolves spatially and temporally during the storm; the reference to a "young" or "old" sea state for each storm characterizes the sea state along the altimeter track during a short period of several minutes and is not representative of the whole storm.

To select the storms, we analyzed tide gauges and JASON-2 altimeter data (Figure 1). The tide gauge database consists of 101 tide gauges in the North Sea, from January 2012 to October 2017 (date of the extraction). The duration of observations depends on sites, and ranges from less than 3 years to more than 5 years. Surges at tide gauges were computed following Eq. 7. The altimeter database covers 8 years (2008-2015) of JASON-2 data along tracks. Surges along tracks were computed following Eq. 8. Analysis of data led to select following storms: ex-Gonzalo, Friedhelm, Felix, and Gunter (Table 1).

The tracks of the 4 selected storms are shown in Figure 2, and the surface winds during the storms are shown in Figure 3. These storms were moving at a speed of around 15 to 20 km/h. In December 2011, Friedhelm crossed the North East Atlantic. Its track is the southernmost one. In the North Sea, the winds are very strong (up to 27 m/s), and the sea state is old, with wave age larger than 1.2 along the altimeter track. In October 2014, ex-Gonzalo reached the Northern part of the British Islands. This storm corresponds to the remnants of Category 4 Atlantic Hurricane Gonzalo. It is the strongest storm in terms of surges, but not in terms of winds (no more than 22.7 m/s). The sea state is young with wave age around 0.9 along the altimeter track. One of the characteristics of this storm is that the strong winds moved from the west to the east as a nearly North-South front of around 1,000 km long (Figure 3 (b)). This explains the discontinuity in the Mean Sea Level Pressure observed in the ex-Gonzalo track over the North Sea, as the minimum moves along this front (red curve on Figure 2). In January 2015, Felix and Gunter crossed the North Atlantic. In fact, three storms succeeded: first Elon, then Felix which crossed the North Sea on the 10th of January, and finally Gunter on the 12th of January 2015. The winds were strong and reached 26.8 m/s (Table 1). For Felix, the sea state was young with wave age close to 0.8 along the altimeter track, whereas for Gunter it was old with wave age larger than 1.2. The old sea for Gunter can be easily explained by the succession of three storms in a short period (few days). The Gunter track was farther north than the Felix one, which may explain why the storm had less impact in term of surges.

3.2. Numerical setup

The ocean model is forced with output from a coupled wave-atmosphere model (Figure 4). Here, we describe the ocean model, the atmosphere model, and the experiments.

3.2.1. Ocean model

We used the default configuration of the TUGO shallow water global ocean model (Lyard et al., 2006), with FES2014 spatial grid (Figure 5). The unstructured space discretization allows the increasing of the resolution in shallow waters, as well as along strong topographic gradient

areas. In the North Sea, the resolution varies from 10-15 km offshore to 4 km along the French and English coasts, and 2 km along the north of the Norwegian coasts. Note that the resolution is not refined in the southeast of the North Sea, due to a lack of detailed bathymetric information in this area (not enough available data).

The ocean model is forced with (1) 10-m wind or (2) surface wind stress from the coupled wave atmosphere model (Figure 4). In the first case (1), the wind stress is computed from the ocean model bulk formula. The drag coefficient is expressed following Hellerman and Rosenstein (1983), which is a wind-only dependent formulation:

$$10^3 C_d = 0.934 + 0.788 \times 10^{-1} U_{10} + 0.868 \times 10^{-1} \Delta T - 0.616 \times 10^{-3} U_{10}^2 - 0.12 \times 10^{-2} \Delta T^2 - 0.214 \times 10^{-2} U_{10} (\Delta T) \quad (9)$$

where U_{10} is the wind at 10 m, and ΔT is the air-sea temperature difference to take into account the stability effect. In the second case (2), the wind stress comes directly from the ECMWF-coupled wave-atmosphere model. Figure 6 shows the TUGO drag for $\Delta T = 0$ and the ECMWF drag, computed over the North Sea during two days for each storm: Fridhelm, ex-Gonzalo, Felix, and Gunter. For winds lower than 15 m/s, the TUGO drag is quite similar to the ECMWF one, but with no variability. For winds stronger than 15 m/s, the TUGO drag is generally lower than the ECMWF one. For a given wind speed, the variability of the ECMWF drag depends on the wave age (Figure 7), even if this dependency is not explicit (see section 3.2.2). Note that the TUGO drag is quite close to the ECMWF drag for old sea state, but lower for young sea state.

3.2.2. Atmosphere model

We used the ECMWF-coupled wave-atmosphere model - IFS (Integrated Forecasting System) - to generate atmospheric forcing (Figure 4). We conducted the simulations without data assimilation. The IFS CY41R1 cycle (ECMWF, 2015a) has a spatial resolution of around 16 km (TL1279) and 137 vertical levels. It has been coupled with the spectral wave model ECWAM (ECMWF Wave Model, ECMWF (2015b)) since 1998. ECWAM uses a coarser horizontal resolution than IFS at around 28 km, with 36 directions and 36 frequencies exponentially spaced, with starting frequency 0.035 Hz and an increment of 1.1. In ECWAM, the source terms are $S = S_{in} + s_{nl} + S_{ds} + S_{bot}$, where S_{in} represents the wind input, S_{nl} represents the nonlinear wave-wave interactions, S_{ds} represents the dissipation due to whitecapping, and S_{bot} represents the bottom friction. The parameterizations of these source terms are discussed in ECMWF (2015b).

The wind stress is represented by classical bulk formulae (Eq. 1). We assume that the wind stress is in the wind direction—that is, the effects of wind-wave misalignment are not accounted here. The drag coefficient is expressed following Janssen (1991), which is a wave-dependent formulation. In neutral conditions, the drag coefficient can be expressed as

$$C_d = \frac{\kappa^2}{\left[\log\left(\frac{10}{z_0}\right)\right]^2} \quad (10)$$

where z_0 is the roughness length, and κ is von Kármán's constant (0.4). The roughness length is expressed as

$$z_0 = \frac{0.11\nu}{u_*} + \alpha \frac{u_*^2}{g} \quad (11)$$

where ν is the kinematic viscosity, and α is the Charnock's parameter (Charnock, 1955). Note that the ECWAM wave model uses Eqs 10 and 11, but Eq. 11 is reduced to the second term, that is, roughness associated with an overall form drag of the wave field; the first term, that is, roughness associated to the viscous properties of the flow, is computed in the IFS atmosphere model. The modification of the roughness length z_0 impacts the drag coefficient and the wind stress (Eqs 10 and 1), then the sea level (Eqs 2 and 3), but also the wind profile. Indeed, when roughness increases, friction also increases, and this slows down the wind (Pineau-Guillou et al., 2018). Janssen (1991) parameterized the quasi-linear wave growth effect as an effective larger Charnock parameter, expressed as a function of the wave-induced stress τ_w

$$\alpha = \frac{\alpha_0}{\sqrt{1-\frac{\tau_w}{\tau}}} \qquad (12)$$

with $\alpha_0 = 0.006$. The wave-induced stress τ_w is the momentum flux transferred from the atmosphere to the waves. It can be related to the wind-wave growth parameter β and the directional wave spectrum $E(f,\theta)$

$$\tau_w = \rho g \int_0^{\infty} \int_0^{2\pi} \beta(f,\theta) E(f,\theta)/(c(f))\, df\, d\theta \qquad (13)$$

where θ is the direction, f is the relative wave frequency, and $c(f)$ is the phase speed, which is a function of frequency (Janssen, 2004). The wave-growth parameter is expressed as $\beta = (\beta_m/\kappa^2)\,\mu \ln^4(\mu), \mu \leq 1$, where β_m is a constant (1.2), and μ is the dimensionless critical height (ECMWF, 2015b). In Eq. 13, the frequency f is integrated from 0 to a high-frequency limit f_c (prognostic part of the wave spectrum) using the discretized spectrum. Beyond f_c (diagnostic part of the wave spectrum), the shape of the spectrum is assumed, and the resulting integral can be evaluated using a simple integration scheme (ECMWF, 2015b). It is assumed that the diagnostic part of the wave spectrum is given as $E(f,\theta) = E(f_c,\theta)(f/f_c)^{-5}$ for $f > f_c$. The high frequency limit f_c is set as $f_c = \min(f_{max}, 2.5 f_{windsea})$, where f_{max} is the maximum discretized frequency, and $f_{windsea}$ is the mean frequency of the modelled wind sea (ECMWF, 2015b).

The ocean model is forced by the atmospheric stress τ. However, a part of the atmospheric stress is going into the waves. The momentum flux going into the ocean τ_{oc} is the sum of two contributions (Figure 8): the part of the atmospheric flux which was not used to generate the waves $\tau_o = \tau - \tau_w$, and the momentum flux transferred from the waves to the ocean by dissipation τ_{diss} (ECMWF, 2015b)

$$\tau_{oc} = \tau_o + \tau_{diss} = \tau - \tau_w + \tau_{diss}. \qquad (14)$$

A more correct approach would be to force the ocean model with τ_{oc} rather than τ. The normalized stress going into the ocean corresponds to the ratio τ_{oc}/τ (output parameter of the ECMWF operational version, but not available in the research version of IFS we used). The normalized stress is lower than 1 when the waves are growing, and greater than 1 when they are dissipating. It is globally close to 1 but can reach values as high as 1.5 under extreme conditions, such as with a passing front (Janssen, 2012). In the ex-Gonzalo case study, it could locally be greater than 2 when the front was passing (Pineau-Guillou, 2018). The strong gradients suggest a potential impact on the ocean model. Curcic (2015) also investigated the ratio between the oceanic and atmospheric stress in tropical cyclones; he found typical values between 0.85 and 1 depending on the wave state.

343
344 *3.2.3. Experiments*
345 We simulated the 4 selected storms (ex-Gonzalo, Friedhelm, Felix, and Gunter) with two stress
346 parameterizations—that is, the wind-dependent and the wave-dependent parametrizations. Note
347 that Felix and Gunter are in the same simulation as they follow each other. For each storm, the
348 model was initialized for at least 15 days, with winds and atmospheric pressure coming from
349 the ECMWF operational 1 h forecasts (i.e. combining hourly operational forecasts computed
350 twice a day at 00:00 and at 12:00). Once initialized, each storm simulation lasted 5 days and
351 was forced by (1) the 10 m-wind or (2) directly by the wind stress, and the atmospheric pressure,
352 with a 1h temporal resolution. In this case, the wind stress comes from the atmosphere model.
353 When forced by the 10 m-wind (1), the drag is a wind-dependent formulation, computed by
354 TUGO (Eq. 9 with $\Delta T = 0$, Hellerman and Rosenstein (1983)), whereas when forced by the
355 wind stress (2), the drag is a wave-dependent formulation, which has seen the waves through
356 IFS/WAM coupling (Eqs 10, 11, 12 and 13, Janssen (1991)).
357
358 *3.3. Validation data*
359
360 Among the 101 tide gauges, 22 tide gauges were selected for comparison with the model (Figure
361 1). The following were the criteria: 1) the tide gauges must have data available during the
362 storms, 2) the tide gauges must open up to the ocean, rather than at the end of a bay, 3) a
363 maximum number of the tide gauges must be offshore, where processes are different from
364 harbors, and 4) a maximum number of tide gauges must be located along the tracks. The
365 JASON-2 tracks with the maximum surges are tracks 170 for Friedhelm, 61 for ex-Gonzalo, 94
366 for Felix, and 170 for Gunter (Figure 1). All the data (tide gauges and JASON-2) were processed
367 as described in section 2.
368
369 **4. Results**
370
371 To investigate the impact of the waves, we compared the surges with wind-dependent
372 (Hellerman and Rosenstein, 1983) and wave-dependent (Janssen, 1991) parameterization
373 during four storms—two with a young sea state (ex-Gonzalo and Felix) and two with an old sea
374 state (Friedhelm and Gunter). Note that Felix and Gunter followed each other, and correspond
375 to the same simulation. We compared the simulated surges with observations, namely tide
376 gauges and JASON-2 altimetric data.
377
378 Figure 9 shows the surge comparison between the model and 3 tide gauges (representative of
379 the whole) for ex-Gonzalo, Felix, and Gunter (no data were available for Friedhelm in 2011, as
380 the CMEMS tide gauge database starts only in 2012); Table 2 summarizes the corresponding
381 errors between the model and the tides gauges: bias, Root Mean Square Error (RMSE), and
382 Peak Error (defined as the difference between the maximum observed and modelled surge).
383 Finally, Figures 10 and 11 show the surge comparison between the model and JASON-2
384 altimetric data, for ex-Gonzalo and Friedhelm. Note that the grey shaded area corresponds to
385 deep waters, where the wind stress effect is lower.
386
387 Analysis of ex-Gonzalo (young sea) and Friedhelm (old sea) gives the following results.
388
389 The first result is that globally, the model matches very well with the observations. For the
390 wave-dependent parameterization, on average, the bias between the model and all the tide
391 gauges is close to zero, the RMSE is 0.12 m, and the Peak Error is -0.09 m (Table 2). The errors
392 between the model and JASON-2 are lower than the errors between the model and the tide

gauges: the bias is close to zero, and the RMSE is 0.08 m, whereas the surge ranges up to 1.40 m (Figure 10). Note also the very good agreement between the model, JASON-2 data, and the tide gauge situated along the track (D151TG, see Figure 1 for the tide gauges location). Unfortunately, the tide gauge Cromer located on the northeast coast of England at the end of the track did not record data during this storm. For Friedhelm, the model also matches the altimeter quite well, but not as well as for ex-Gonzalo. For the wave-dependent parameterization, the bias and RMSE reach -0.12 m and 0.08 m, respectively (Figure 11). The differences could be due to uncertainties in altimeter corrections, such as geophysical corrections (for example tide). However, note that the agreement between the model and the altimeter is very good in shallow waters, where the wind stress effect is the most significant (Figure 11 (b)). To conclude, the errors between the model and the observations (tide gauges and altimeter data) for these two storms are small enough to confirm the capability of a global model to accurately predict storm surges, even in the coastal areas, when its spatial resolution is fine enough to catch the storm size. These results also confirm the capability of altimeters to accurately measure surges (Antony et al., 2014).

The second result is that the wave-dependent parameterization yields higher surges only when the sea state is young (ex-Gonzalo, Figures 9 (a) and 10 (b)). Otherwise, the surges are similar, regardless of the parameterization (Friedhlem, Figure 11 (b)). Physically, this is not surprising as old sea corresponds to a situation where waves are no longer rapidly growing resulting in sharp reduction of the momentum flux from the atmosphere to the waves. When the sea state is old, the drag coefficients from the two parameterizations are close to each other (Figure 7), and the surges are then similar. However, in the presence of young and steep waves, the drag increases with Janssen's parameterization due to higher values of the Charnock parameter (Figure 12 (c) and (d)). This yields higher drag than the wind-dependent formulation, and later higher wind stress (Figure 12 (e) and (f)) and higher surges. The differences between these two parameterizations corresponds to the effect of the waves on the surges. This difference reaches 25 cm at Lowestoft (Figure 9 (a)) and 20 cm along Jason-2 track (Figure 10 (b)). We note the very good agreement in terms of Significant Wave Height (SWH) between the ECMWF coupled wave-atmosphere model and JASON-2 altimeter (Piolle et al., 2019) for ex-Gonzalo (Figure 12 (b) and 13 (b)), and for Gunter (Figure 13 (d)). The very strong SWH gradient along the track for ex-Gonzalo corresponds to the passage of the front (Figure 13 (b)).

The third result is that the wave-dependent parameterization is closer to the observations than the wind dependent one. These results are consistent with those previously obtained by Mastenbroek et al. (1993), Nicolle et al. (2009), and Bertin et al. (2015). Along the JASON-2 track, the RMSE is reduced from 0.13 m to 0.08 m (Figure 10 (b)). On average, in the 21 tide gauges, the Peak Error is reduced from -0.21 m to -0.09 m (Table 2). However, in some tide gauges, the surges are still underestimated. The tides gauges can be separated into three groups:

- Group 1: a first group of 11 tide gauges (in blue in Figure 1), where the surges with the wave-dependent stress match well with observations, such as Lowestoft and EuroplatformTG in Figure 9 (a). This corresponds to the 4 offshore tide gauges (F3platformTG, D151TG, EuroplatformTG, VlakteVdRaanTG) as well as 7 other tide gauges onshore.
- Group 2: a second group of 5 tide gauges (in green in Figure 1), where the surges with the wave-dependent stress are still underestimated, such as Whitby in Figure 9 (a).
- Group 3: a third group of 5 tide gauges (in black in Figure 1), where the effect of the parameterization is not significant; this corresponds to tide gauges located in the northern part of the North Sea, where surges are smaller than 0.50 m. In this part, the bathymetry ranges from 50 to 200 m, and the effect of wind stress is smaller than in the

southern part, with shallow waters. That may explain the non-significant differences between the two parameterizations.

Note that in the second group where surges are still underestimated, there are no tide gauges offshore. This underestimation is probably partly due to processes taking place in the very nearshore, and not modelled by TUGO (e.g. wave setup, see the discussion in section 5). This could suggest that comparisons with the altimeter are better, as the tracks offshore are not contaminated by coastal processes such as wave setup. Another reason that could explain this negative bias is the lack of spatial resolution near the coast (only 2 km). Experiments show that atmospheric surges may increase from 0.1 to 0.3 between 10 m isobath and the shoreline (personal communication from X. Bertin); here, the spatial resolution is not fine enough to correctly represent this increase.

After the analysis of ex-Gonzalo (young sea) and Friedhelm (old sea), analysis of Felix (young sea) and Gunter (old sea) give partly similar results. (1) The model still matches quite well with the tide gauges (bias, RMSE, and Peak Error are respectively 0 cm, 19 cm, and -10 cm for the wave-dependent parameterization; see Table 2). (2) The wave-dependent parameterization still yields to higher surges when the sea state is young. The impact of the waves on the surges reaches around 11 cm at Europlatform and around 20 cm along Jason-2 track (not shown). (3) We find also that the wave-dependent parameterization is closer to the tide gauge observations, reducing on average the Peak Error from -0.14 m to -0.10 m. However, comparison between the model and the altimeter is not as good as for ex-Gonzalo and Friedhelm (not shown), and it is difficult to conclude which parameterization is the most appropriate. This suggests that the number of case studies should be increased, to give more confidence in our conclusions.

5. Discussion

Here, we discuss the influence of the wind direction, the processes contributing to the surges, and the impact on the altimetric corrections.

5.1. Impact of the wind direction

Analysis of tide gauge and altimeter data revealed that ex-Gonzalo was the storm with the highest surge, whereas it was the one with the weakest winds (only 23 m/s in the North Sea, against 27 m/s for Friedhelm, see Table 1). This is mainly due to the wind direction. Figure 14 shows wind roses in the middle of the North Sea (4°E 56°N), during the 5-day simulations of the storms. For ex-Gonzalo (Figure 14 (a)), strong winds were mainly from the northwest direction, pushing the waters along the southern coast of the North Sea, whereas for other storms, strong winds came mainly from the west (see also Figure 3).

This is probably not the only explanation for ex-Gonzalo high surges. The track of this storm is the southernmost one; the storm crosses the south of the North Sea, and the shallow waters may enhance the wind stress contribution.

5.2. Processes contributing to the surges

Even if the wave-dependent parameterization yields higher surges, the modelled surges are still underestimated compared with some tide gauges (5 over 21 for ex-Gonzalo storm). The comparison between modelled and observed surges is complicated by the different processes that contribute to the surge and that are not always modelled (see Table 3). Generally, the dominant effect is the atmospheric forcing (Mean Sea Level Pressure and winds). This

contribution is commonly of the order of 50 cm, but can exceed 1 m in severe storms and hurricanes, as in the case of Xynthia in February 2010 at La Rochelle (Pineau-Guillou et al., 2012; Bertin et al., 2012). In case of progression in very shallow waters, as for example in the South of the North Sea, the surges can reach up to 2 or 3 m. This atmospheric contribution is taken into account in the ocean model through the atmospheric forcing.

Another important contribution to the total surge - which is here not taken into account - is the wave setup, that is, the surge due to wave dissipation (mainly by wave breaking) in the nearshore areas (Bunya et al., 2010; Kim et al., 2010; Brown et al., 2010; Idier et al., 2012; Lee et al., 2013; Bertin et al., 2015; Thuy et al., 2017; Choi et al., 2018). To model the wave setup, the radiation stress has to be introduced. The radiation stress is the momentum flux carried by the waves. When the waves dissipate, such as by wave breaking or strong bottom friction, this generates nearshore currents and an additional surge, the wave setup. Its contribution to the total surge may be significant. For instance, values of 0.5 to 1.5 m were reported in Liverpool Bay (Brown et al., 2010), more than 0.5 m (i.e. 50% or more of the total surge) in the southern part of the Bay of Biscay (Idier et al., 2012), and 10 to 20 cm in the central part of the Bay of Biscay (Bertin et al., 2015). In coastal areas, it can contribute up to 80% of the total storm surge (Pedreros et al., 2018). During typhoons, it can contribute up to 15% following Thuy et al. (2017) and even 40% following Kim et al. (2010). In the North Sea, Choi et al. (2018) reported contributions of around 20 cm and 10% of the total surge during 1953 Big Flood. To capture the wave setup well, (1) the ocean model has to be coupled one-way or two-way with a wave model to take into account the radiation stress, and (2) the grid spatial resolution has to be high enough, that is, around 10 m. As a consequence, due to a too coarse grid (3 to 15 km in the North Sea), the wave setup is not modelled in this study (as is generally done in global and regional models). This is a limitation for comparison with coastal tide gauges, but not with altimeter, as wave setup is close to zero far from the coast. Note that the present study would benefit from more tide gauge observations offshore (where wave setup is negligible).

Other contributions are the waves whose signature may be significant at the surface when propagating in coastal areas, such as meteo-tsunami, infragravity waves - only few cm in deep ocean (Aucan and Ardhuin, 2013) but can reach more than 1 m in coastal areas (Sheremet et al., 2014), internal solitary waves (can reach 20 cm in coastal areas) as well as internal waves, rogue waves, and tsunamis - surge due to an earthquake, landslide, or volcanic eruption. Finally, seiches - resonance phenomena in closed or semi-closed basins - also contribute to the surges. Their amplitude can be significant in harbors and sometimes reach several tens of centimeters.

5.3. Impact on the altimetric corrections

The accuracy of the simulated storm surges is essential, as it directly impacts the accuracy of Sea Level Anomaly products through the Dynamic Atmospheric Correction (Eq. 8). Figure 15 shows the differences between the default SLA from CTOH (blue curve) and the new reconstructed one (red curve) with the DAC taking into account the waves, that is, from the TUGO simulation forced with the ECMWF wind stress. The new reconstructed SLA is on average closer to zero. The SLA has been improved by removing some surge residual due to atmospheric effect. The difference between the two SLA (the native and the reconstructed one) reaches 40 cm near the coast. Note that in this 40 cm, around 20 cm may be attributed to the waves impact, and the other 20 cm are probably due to a better ocean model resolution and a better temporal atmospheric forcing (1h versus 6h in the DAC product from CTOH).

6. Conclusions

We investigated the impact of a wave-dependent stress on surge modelling. During ex-Gonzalo and Friedhelm storms, which are characterized respectively by young and old sea states, we compared simulated surges with wind-dependent and wave-dependent stress (Hellerman and Rosenstein, 1983; Janssen, 1991). We compared the results with tide gauges and altimetric data.

We showed that the global ocean model accurately predicts storm surges in coastal areas (RMSE of 0.12 m). This can be attributed partly to the unstructured grid, which allows increasing the resolution in the shallow waters. The consistency between the model, the altimeter, and the tide gauges also confirms the capability of altimeters to accurately measure surges (RMSE of 0.08 m along the track).

We showed that when the sea state is old, the wind-dependent formulation Hellerman and Rosenstein (1983) is appropriate. However, when the sea becomes younger and rougher, the wind stress increases, and a wave-dependent formulation (here, Janssen (1991)) is more appropriate. This reduces the Peak Error significantly (e.g. from 0.21 m to 0.09 m). The waves effect on the surge can reach 20 to 25 cm. This result is consistent with previous studies (Mastenbroek et al., 1993; Nicolle et al., 2009; Bertin et al., 2015). However, the number of case studies should be increased to confirm these conclusions. Indeed, taking into the waves allows to obtain surges closer to observations, but could be a way to compensate other errors. For example, Moon et al. (2009) concluded that Mastenbroek et al. (1993) obtained good simulated surges with overestimated drag by compensating surge error due to a too coarse grid.

This work underlines the lack of consistency of the drag between the wave, atmosphere, and ocean models (van Nieuwkoop et al., 2015). One recommendation could be to force the ocean model with the wind stress from a coupled wave-atmosphere model, which has seen the waves (e.g. ECMWF model). This would yield to (1) more consistency between the drag from the ocean and the atmosphere models and (2) improvement of the storm surges taking into account the wave effect. To go even further, we would recommend forcing the ocean model with the stress going into the ocean τ_{oc} rather than the atmospheric stress τ.

In this study, we showed that the ocean model better matches with tide gauges offshore (compared with onshore) and altimeter tracks. This is probably due to coastal effects in tide gauges (e.g. wave setup) that are not modelled in the TUGO ocean model and that are not seen with the altimeters (as the tracks are offshore). This suggests that tide gauges should not always be considered as a reference, and that what we generally call "errors" between model/tide gauges or altimeter/tide gauges also includes local coastal processes. Consequently, we should not always want the model (or altimeter) to match perfectly with tide gauges.

Finally, we should mention several limitations in this study. (1) Results are specific to the ECMWF and TUGO parameterizations used here (Janssen, 1991; Hellerman and Rosenstein, 1983). (2) The wind stress is mainly supported by the capillary and short gravity waves, that is, the tail of the spectrum, which is crudely represented in wave models today (Kudryavtsev et al., 2014; Peureux and Ardhuin, 2016). Dedicated efforts are being made to improve wave breaking parameterization, in order to also improve the tail of the spectrum. There are also many uncertainties of the wave growth parameter β. (3) We assume that the wind stress is in the wind direction, as it is mainly supported by high-frequency waves which respond quickly to changes in the wind direction (Janssen, 2004). Possible wind-wave misalignment is not accounted here. (4) The ocean model is forced by the atmospheric stress τ, whereas a more correct approach would be to force it with the stress going into the ocean τ_{oc}. (5) The wave

setup, that is, the surge generated by the wave dissipation (e.g. wave breaking), is not accounted here. It may reach up to 20 cm in the North Sea (Choi et al., 2018). (6) We have investigated the wind stress sensitivity on the surges, but other factors impact the surges, such as grid spatial resolution, bottom friction, bathymetry, and coastal geometry (Mao and Xia, 2017). Despite we obtain modelled surges closer to the observations, there are still some possible compensation of errors due to uncertainties on other modelling terms. Note that we did not go further in investigating how these other factors may impact the surge dynamics, as this is not within the scope of the present paper. (7) The ocean model is here forced by the atmosphere model. Two-way ocean-atmosphere coupling would probably affect the resulting water levels, as both the wind U_{10} and the atmospheric stress τ will be modified to account for the moving ocean surface (Hersbach and Bidlot, 2009).

Acknowledgment

Acknowledgement is made for the use of ECMWF's computing and archive facilities in this research. We thank all ECMWF staff for the warm welcome and excellent support provided. We thank CMEMS for providing tide gauges data. We also thank CTOH/LEGOS for providing JASON-2 1Hz X-track coastal product, LEGOS for providing TUGO ocean model, and ESA Sea State Climate Change Initiative and Ifremer for providing JASON-2 Significant Wave Height. We also warmly thank Xavier Bertin and Michel Benoit for their constructive comments and suggestions. Finally, the authors would like to thank the reviewers for their careful reading and their constructive comments, which allowed us to improve this article.

Figure 1: Tide gauges and JASON-2 tracks. The tracks numbered 094, 170, and 061 are the ones with maximum surges for storms Felix, Friedhelm/Gunter, and ex-Gonzalo (see Table 1). The 4 groups of tide gauges correspond to the 22 tide gauges used for this study. For ex-Gonzalo storm, group 1 matches quite well with observations, group 2 shows an underestimation, group 3 is not sensitive to the parameterization (deep waters), and group 4 has no data during this storm.

Figure 2: Tracks of the minimum of the Mean Sea Level Pressure for the selected storms (from ECMWF simulations). The asterisk on the figure corresponds to the time for the wind plot (Figure 3).

Figure 3: 10 m winds during the storms (a) Friedhelm, 8 December 2011, 22:00 (b) ex-Gonzalo, 21 October 2014, 17:00 (c) Felix, 10 January 2015, 10:00 (d) Gunter, 12 January 2015, 17:00 (from ECMWF simulations).

Figure 4: Ocean model forced with a coupled wave-atmosphere model.

Figure 5: FES2014 grid over the North East Atlantic.

Figure 6: Comparison of drag coefficient for the TUGO parameterization (Hellerman and Rosenstein, 1983) and the ECMWF (CY41R1) parameterization. For the ECMWF model, computation is made over the North Sea over two days.

Figure 7: Comparison of drag coefficient for the TUGO parameterization (Hellerman and Rosenstein, 1983) and the ECMWF (CY41R1) parameterization. Vertical bars correspond to one standard deviation. For the ECMWF model, computation is made over the North Sea over two days.

Figure 8: Schematic representation of momentum fluxes at the air-sea interface (adapted from Janssen et al. (2013)). The momentum flux going into the ocean τ_{oc} is the sum of τ_o and τ_{diss}.

Figure 9: Observed and modelled surges with two parameterizations (wind- and wave-dependent) at tide gauges Lowestoft, EuroplatformTG, and Whitby during (a) ex-Gonzalo, (b) Felix, and (c) Gunter storms.

Figure 10: Surges from TUGO model, JASON-2 altimeter, and tide gauges during ex-Gonzalo (young sea) (a) over the North Sea (b) along Jason-2 track. The grey shaded area corresponds to deep waters (>100 m), where wind stress effect is lower.

Figure 11: Surges from TUGO model and JASON-2 altimeter during Friedhelm (old sea) (a) over the North Sea (b) along Jason-2 track. The grey shaded area corresponds to deep waters (>100 m), where wind stress effect is lower.

Figure 12: (a) Wind, (b) Significant Wave Height (SWH), (c) Wave age, (d) Charnock parameter, (e) wind stress from the ECMWF coupled wave-atmosphere model, and (f) wind stress from TUGO ocean model, during ex-Gonzalo storm (young sea), October 21 2014, 23:00. The colored dots on (b) correspond to the observed Significant Wave Height from JASON-2 altimeter.

Figure 13: Significant Wave Height from JASON-2 altimeter and the ECMWF model during (a) Friedhlem, (b) ex-Gonzalo, (c) Felix, and (d) Gunter storms.

Figure 14: Wind roses (m/s) in the middle of the North Sea (4°E 56°N) during the 5-day simulations of storms (a) Friedhelm (b) ex-Gonzalo (c) Felix/Gunter. The color corresponds to the wind speed (in m/s), and the bar size corresponds to the distribution (in %).

Figure 15: Comparison of default SLA (blue curve) and reconstructed SLA (red curve) taking into account the waves for track 061 during ex-Gonzalo.

Name	Track date	Track number	Type of sea state	Rank from JASON-2 analysis	Rank from TGs analysis	Max. wind (m/s)
Friedhelm	2011-12-10 02:43	170	old sea	5	/	27.0
ex-Gonzalo	2014-10-21 22:39	061	young sea	2	1	22.7
Felix	2015-01-10 12:44	94	young sea	6	5	26.8
Gunter	2015-01-13 11:55	170	old sea	20	/	25.5

Table 1: Storms selected for this study. The type of sea state (column 4) indicates if the sea state is young or old along the track. The rank (columns 5 and 6) corresponds to maximum surges. Maximum winds (column 7) are computed over the North Sea (4°E 10°W 50°N 65°N) during two days from the ECMWF simulations.

Tide Gauge	Bias (m) Wind-dep.	Bias (m) Wave-dep.	RMSE (m) Wind-dep.	RMSE (m) Wave-dep.	Peak Err. (m) Wind-dep.	Peak Err. (m) Wave-dep.
EX-GONZALO						
Group 1						
D151TG	0.007	0.002	0.084	0.070	-0.124	-0.024
EuroplatformTG	0.016	0.024	0.130	0.120	-0.165	0.061
F3platformTG	0.007	0.000	0.084	0.061	-0.129	-0.005
Harwich	-0.068	-0.045	0.161	0.155	-0.169	0.106
IjmuidenTG	0.022	-0.001	0.192	0.162	-0.336	-0.175
Leith	-0.018	-0.012	0.119	0.114	-0.141	-0.080
Lowestoft	-0.029	-0.028	0.126	0.111	-0.307	-0.077
StavangerTG	0.018	-0.003	0.095	0.072	-0.103	-0.024
TregdeTG	0.011	-0.005	0.126	0.106	-0.248	-0.146
VlakteVdRaanTG	-0.012	-0.015	0.160	0.163	-0.161	0.047
Whitby	-0.005	-0.021	0.106	0.095	-0.234	-0.147
Group 2						
DunkerqueTG	-0.020	-0.041	0.189	0.181	-0.473	-0.319
HelgolandTG	0.083	0.072	0.202	0.173	-0.433	-0.207
HoernumTG	0.103	0.071	0.230	0.184	-0.437	-0.219
NorderneyTG	0.029	-0.000	0.261	0.218	-0.539	-0.328
VlielandHavenTG	0.014	-0.009	0.201	0.174	-0.374	-0.224
Group 3						
Aberdeen	0.026	0.011	0.084	0.074	-0.026	-0.003
Lerwick	0.010	0.015	0.038	0.038	-0.007	-0.004
MaloyTG	0.031	0.009	0.064	0.052	-0.065	-0.041
NorthCormorantTG	0.039	0.036	0.052	0.048	0.028	0.026
Wick	0.030	0.003	0.078	0.065	0.014	-0.026
Group 4						
Cromer	-	-	-	-	-	-
Mean	**0.014**	**0.003**	**0.132**	**0.116**	**-0.211**	**-0.086**
FELIX/GUNTER Mean	**0.011**	**0.001**	**0.198**	**0.190**	**-0.138**	**-0.104**

Table 2: Bias, RMSE, and Peak Error for wind- and wave-dependent parameterization during the 5-day simulation for ex-Gonzalo and Felix/Gunter storms. For ex-Gonzalo, Group 1 matches quite well with observations (see the

681 last column for the Peak Error), Group 2 shows an underestimation (see also the last column for the Peak Error),
682 Group 3 is not sensitive to the parameterization (deep waters), and Group 4 has no data during this storm. See
683 Figure 1 for the location of the 4 groups.
684

Process	Location	Computed in hydrodynamic models
Atmospheric surge due to wind and atm. pressure	Everywhere	Yes, if atmospheric forcing is introduced
Wave setup, i.e. surge due to wave breaking	In nearshore areas	Yes, if resolution is fine enough, and if radiation stress is introduced
Tide surge interaction	Significant in very shallow waters	Yes, if meteorological and tide forcing are introduced
Meteo-tsunami		Yes, if the space resolution is fine enough
Infragravity waves		Yes, if the hydrodynamic model is coupled with a wave model
Internal waves	Everywhere	Yes, in a baroclinic model
Rogue waves		No
Tsunamis i.e. surge due to an earthquake, landslide, or volcanic eruption		No
Seiches i.e. resonance phenomena in closed or semi-closed basins	Mainly in harbors or bays	Yes, if the spatial resolution is fine enough; this is rarely the case in global or regional models

685
686 Table 3: Various processes contributing to the surge
687
688

References

Allain, D. J., 2013. TUGOm tidal toolbox. Tech. rep., LEGOS Documentation.

Andreas, E. L., 2009. Relating the drag coefficient and the roughness length over the sea to the wavelength of the peak waves. J. Phys. Oceanogr. 39, 3011-3020.

Antony, C., Testut, 470 L., Unnikrishnan, A., 2014. Observing storm surges in the Bay of Bengal from satellite altimetry. Estuarine, Coastal and Shelf Science 151, 131-140.

Aucan, J., Ardhuin, F., 2013. Infragravity waves in the deep ocean: An upward revision. Geophys. Res. Lett. 40, 3435-3439.

Bertin, X., Bruneau, N., Breilh, J.-F., Fortunato, A. B., Karpytchev, M., 2012. Importance of wave age and resonance in storm surges: The case Xynthia, Bay of Biscay. Ocean Modelling 42, 16-30.

Bertin, X., Li, K., Roland, A., Bidlot, J.-R., 2015. The contribution of short-waves in storm surges: Two case studies in the Bay of Biscay. Continental Shelf Research 96, 1-15.

Birol, F., Fuller, N., Lyard, F., Cancet, M., Niño, F., Delebecque, C., Fleury, S., Toublanc, F., Melet, A., Saraceno, M., Léger, F., 2016. Coastal applications from nadir altimetry: Example of the X-TRACK regional products. Advances in Space Research 59 (4), 936-953.

Black, P. G., D'Asaro, E. A., Drennan, W. M., French, J. R., Niller, P. P., Sanford, T. B., Terrill, E. J., Walsh, E. J., Zhang, J. A., 2007. Air-sea exchange in hurricanes: Synthesis of observations from the coupled boundary layer airsea transfer experiment. Bull. Amer. Meterol. Soc. 88, 359374.

Brown, J. M., Souza, A. J., Wolf, J., 2010. An investigation of recent decadal-scale storm events in the eastern Irish Sea. J. Geophys. Res. 115, C05018.

Bunya, S., Dietrich, J., Westerink, J., Ebersole, B., Smith, J., Atkinson, J., Jensen, R., Resio, D., Luettich, R., Dawson, C., Cardone, V., Cox, A., Powell, M., Westerink, H., Roberts, H., 2010. A high resolution coupled riverine, tide, wind, wind wave, and storm surge model for southern Louisiana and Mississippi: Part I model development and validation. Mon. Weather Rev. 138, 345-377.

Carrère, L., Lyard, F., 2003. Modeling the barotropic response of the global ocean to atmospheric wind and pressure forcing - comparisons with observations. Geophys. Res. Lett. 30 (6), 1275.

Carrère, L., Lyard, F., Cancet, M., Guillot, A., Apr. 2015. FES 2014, a new tidal model on the global ocean with enhanced accuracy in shallow seas and in the Arctic region. In: EGU General Assembly Conference Abstracts. Vol. 17 of EGU General Assembly Conference Abstracts. p. 5481.

Charnock, H., 1955. Wind stress on a water surface. Quart. Journ. Roy. Meteorol. Soc. 81, 639-640.

Choi, B. H., Kim, K. O., Yuk, J.-H., Lee, H. S., 2018. Simulation of the 1953 storm surge in the North Sea. Ocean Dynamics 6, 1759-1777.

Curcic, M., 2015. Explicit Air-Sea Momentum Exchange in Coupled Atmosphere-Wave-Ocean Modeling of Tropical Cyclones. Open Access Dissertations. 1512. PhD manuscript. 196 p.

Donelan, M. A., Haus, B. K., Reul, N., Plant, W. J., Stiassnie, M., Graber, H. C., Brown, O. B., Saltzman, E. S., 2004. On the limiting aerodynamic roughness of the ocean in very strong winds. Geophys. Res. Lett. 31, L18306.

ECMWF, 2015a. IFS Documentation CY41R1. ECMWF Book.

ECMWF, 2015b. IFS Documentation CY41R1. Part VII: ECMWF Wave Model. ECMWF Book Chapter.

Edson, J. B., Jampana, V., Weller, R. A., Bigorre, S. P., Plueddemann, A. J., Fairall, C. W., Miller, S. D., Mahrt, L., Vickers, D., Hersbach, H., 2013. On the exchange of momentum over the open ocean. J. Phys. Oceanogr. 43, 1589-1610.

739 Hellerman, S., Rosenstein, M., 1983. Normal monthly wind stress over the world ocean with
740 error estimates. J. Phys. Oceanogr. 13 (7), 1093-1104.
741 Hersbach, H., Bidlot, J.-R., 2009. The relevance of ocean surface current in the ECMWF
742 analysis and forecast system. In: ECMWF Workshop on Ocean-Atmosphere Interactions, 10-
743 12 November 2008. ECMWF, pp. 61-73. URL https://www.ecmwf.int/node/9866
744 Holthuijsen, L. H., Powell, M. D., Pietrzak, J. D., 2012. Wind and waves in extreme hurricanes.
745 J. Geophys. Res. 117, C09003.
746 Idier, D., Muller, H., Pedreros, R., Thiebot, J., Yates, M., Creach, R., Voineson, G., Dumas, F.,
747 Lecornu, F., Pineau-Guillou, L., Ohl, P., Paradis, D., 2012. Système de prévision de surcotes
748 en Manche/Atlantique et Méditerranée : Amélioration du système existant sur la façade
749 Manche/Gascogne [D4] . Tech. rep., BRGM/RP-61019-FR.
750 Janssen, P., 2004. The interaction of ocean waves and wind. Cambridge University Press,
751 Cambridge, UK.
752 Janssen, P., 2012. Ocean wave effects on the daily cycle in SST. J. Geophys. Res. 117, C00J32.
753 Janssen, P. A., Breivik, O., Mogensen, K., Vitart, F., Balmaseda, M., Bidlot, J.-R., Keeley, S.,
754 Leutbecher, M., Magnusson, L., Molteni., F., 2013. Air-sea interaction and surface waves.
755 Tech. rep., ECMWF Technical Memorandum 712.
756 Janssen, P. A. E. M., 1991. Quasi-linear theory of wind wave generation applied to wave
757 forecasting. J. Phys. Oceanogr. 21, 1631-1642.
758 Jarosz, E., Mitchell, D. A., Wang, D. W., Teague, W. J., 2007. Bottom-up determination of air-
759 sea momentum exchange under a major tropical cyclone. Science 315, 1707-1709.
760 Kim, S. Y., Yasuda, T., Mase, H., 2010. Wave set-up in the storm surge along open coasts
761 during Typhoon Anita. Coastal Eng. 57, 631-642.
762 Kudryavtsev, V., Chapron, B., Makin, V., 2014. Impact of wind waves on the airsea fluxes: A
763 coupled model. J. Geophys. Res. Oceans 119, 1217-1236.
764 Lee, H. S., Yamashita, T., Hsu, J. R.-C., Ding, F., 2013. Integrated modeling of the dynamic
765 meteorological and sea surface conditions during the passage of Typhoon Morakot. Dynamics
766 of Atmospheres and Oceans 59, 1-23.
767 Lyard, F., Lefevre, F., Letellier, T., Francis, O., 2006. Modelling the global ocean tides: modern
768 insights from FES2004. Ocean Dynamics 56, 394-415.
769 Lynch, D., Gray, W., 1979. A wave equation model for finite element tidal computations.
770 Computers and Fluids 7, 207-228.
771 Mao, M., Xia, M., 2017. Dynamics of wave-current-surge interactions in Lake Michigan: A
772 model comparison. Ocean Modelling 110, 1-20.
773 Mastenbroek, C., Burgers, G., Janssen, P. A. E. M., 1993. The dynamical coupling of a wave
774 model and a storm surge model through the atmospheric boundary layer. J. Phys. Oceanogr. 23,
775 1856-1867.
776 Moon, I.-J., Ginis, I., Hara, T., Thomas, B., 2007. A physics-based parameterization of airsea
777 momentum flux at high wind speeds and its impact on hurricane intensity predictions. Mon.
778 Weather Rev. 135 (8), 2869-2878.
779 Moon, I.-J., Kwon, J.-I., Lee, J.-C., Shim, J.-S., Kang, S. K., Oh, I. S., Kwon, S. J., 2009. Effect
780 of the surface wind stress parameterization on the storm surge modeling. Ocean Modelling 29,
781 115127.
782 Nicolle, A., Karpytchev, M., Benoit, M., 2009. Amplification of the storm surges in shallow
783 waters of the Pertuis Charentais (Bay of Biscay, France). Ocean Dynamics 59, 921-935.
784 Pedreros, R., Idier, D., Muller, H., Lecacheux, S., Paris, F., Yates-Michelin, M., Dumas, F.,
785 Pineau-Guillou, L., Sénéchal, N., 2018. Relative contribution of wave setup to the storm surge:
786 Observations and modeling based analysis in open and protected environments (Truc Vert
787 beach and Tubuai island). Journal of Coastal Research 85, 1046-1050.

Peng, S., Li, Y., 2015. A parabolic model of drag coefficient for storm surge simulation in the South China Sea. Nature Scientific Reports 5, 15496.
Peureux, C., Ardhuin, F., 2016. Ocean bottom pressure records from the Cascadia array and short surface gravity waves. J. Geophys. Res. 121, 28622873.
Pineau-Guillou, L., 2018. Ocean-Atmosphere interaction: improvement of wind stress for coastal physical modelling. PhD manuscript. 140 p.
Pineau-Guillou, L., Ardhuin, F., Bouin, M.-N., Redelsperger, J.-L., Chapron, B., Bidlot, J.-R., Quilfen, Y., 2018. Strong winds in a coupled wave-atmosphere model during a North Atlantic storm event: evaluation against observations. Quart. Journ. Roy. Meteorol. Soc. 144, 317-332.
Pineau-Guillou, L., Lathuiliere, C., Magne, R., Louazel, S., Corman, D., Perherin, C., 2012. Sea levels analysis and surge modelling during storm Xynthia. European Journal of Environmental and Civil Engineering 16 (8), 943-952.
Piolle, J.-F., Dodet, G., Ash, E., Ardhuin, F., 2019. Sea State CCI Product User Guide Version 1.0. Tech. rep., ESA Climate Change Initiative Sea State project.
Powell, M. D., Vickery, P. J., Reinhold, T. A., 2003. Reduced drag coefficient for high wind speeds in tropical cyclones. Nature 422, 279-283.
Sheremet, A., Staples, T., Ardhuin, F., Suanez, S., Fichaut, B., 2014. Observations of large infragravity wave runup at Banneg Island, France. Geophys. Res. Lett. 41 (3), 976-982.
Simon, B., 2007. La marée océanique côtière. Institut Océanographique Editeur, Paris, France.
Takagaki, N., Komori, S., Suzuki, N., Iwano, K., Kuramoto, T., Shimada, S., Kurose, R., Takahashi, K., 2012. Strong correlation between the drag coefficient and the shape of the wind sea spectrum over a broad range of wind speeds. Geophys. Res. Lett. 39, L23604.
Thuy, N. B., Kim, S., Chien, D. D., Dang, V. H., Cuong, H. D., Wettre, C., Hole, L. R., 2017. Assessment of storm surge along the coast of central Vietnam. Journal of Coastal Research 33 (3), 518-530.
van Nieuwkoop, J., Baas, P., Caires, S., Groeneweg, J., 2015. On the consistency of the drag between air and water in meteorological, hydrodynamic and wave models. Ocean Dynamics 65 (7), 989-1000.

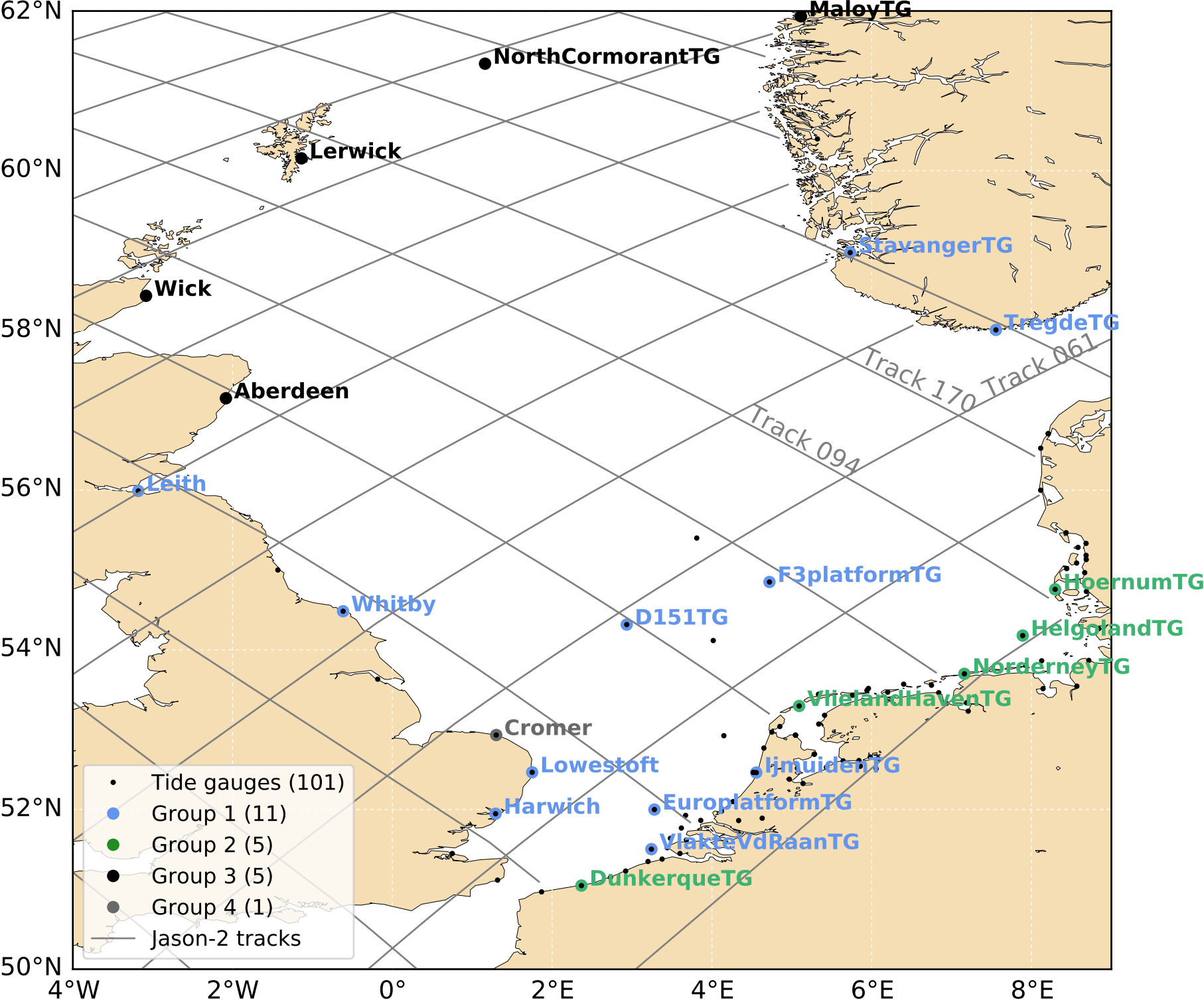
MaloyTG
NorthCormorantTG
Lerwick
StavangerTG
Wick
TregdeTG
Track 170
Track 061
Aberdeen
Track 094
Leith
F3platformTG
HoernumTG
Whitby
D151TG
HelgolandTG
NorderneyTG
VlielandHavenTG
Cromer
Lowestoft
IjmuidenTG
Harwich
EuroplatformTG
VlakteVdRaanTG
DunkerqueTG
Tide gauges (101)
Group 1 (11)
Group 2 (5)
Group 3 (5)
Group 4 (1)
Jason-2 tracks
62°N
60°N
58°N
56°N
54°N
52°N
50°N
4°W
2°W
0°
2°E
4°E
6°E
8°E

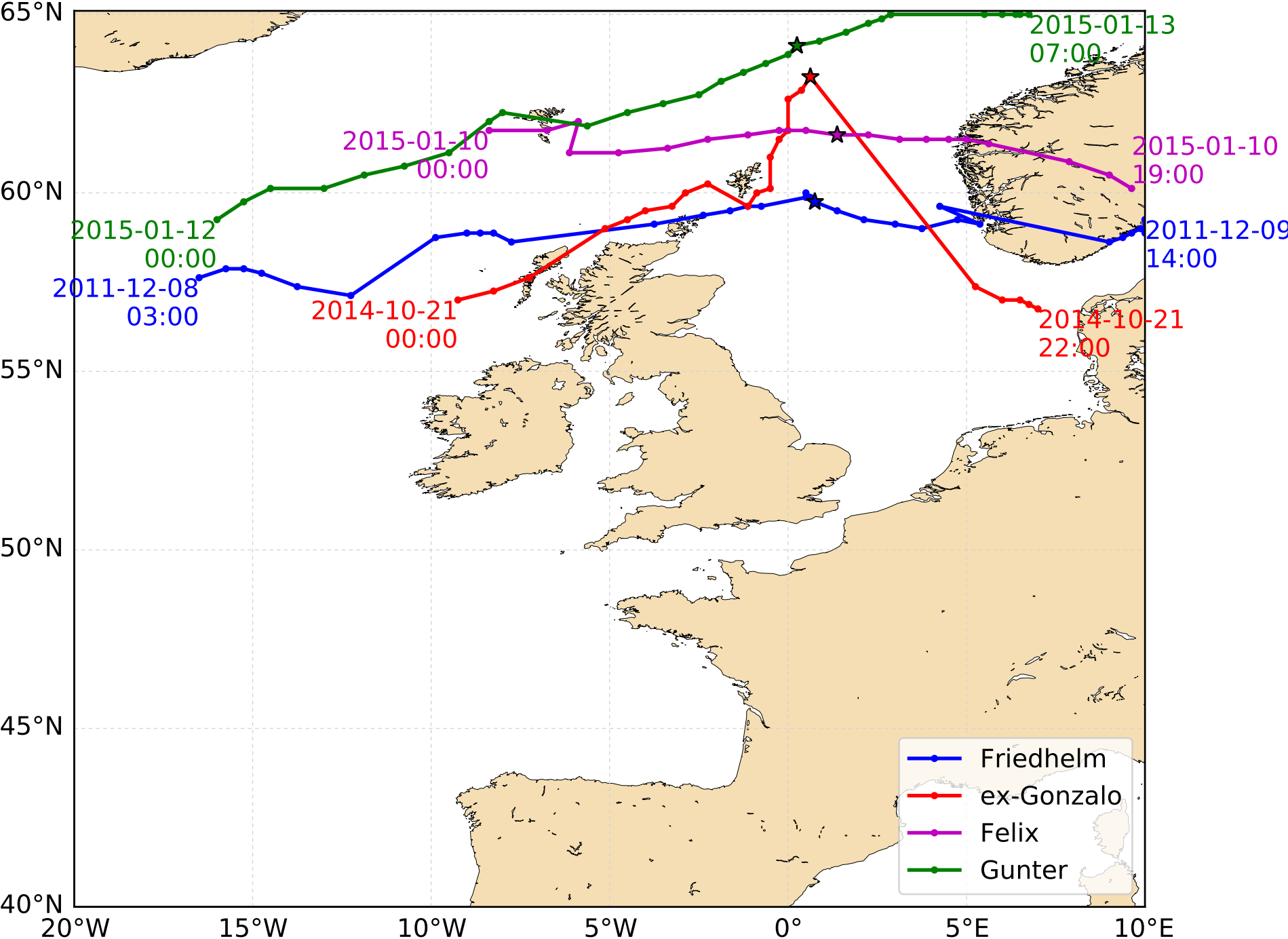
65°N
60°N
55°N
50°N
45°N
40°N
20°W
15°W
10°W
5°W
0°
5°E
10°E
2015-01-13
07:00
2015-01-10
00:00
2015-01-10
19:00
2015-01-12
00:00
2011-12-09
14:00
2011-12-08
03:00
2014-10-21
00:00
2014-10-21
22:00
Friedhelm
ex-Gonzalo
Felix
Gunter

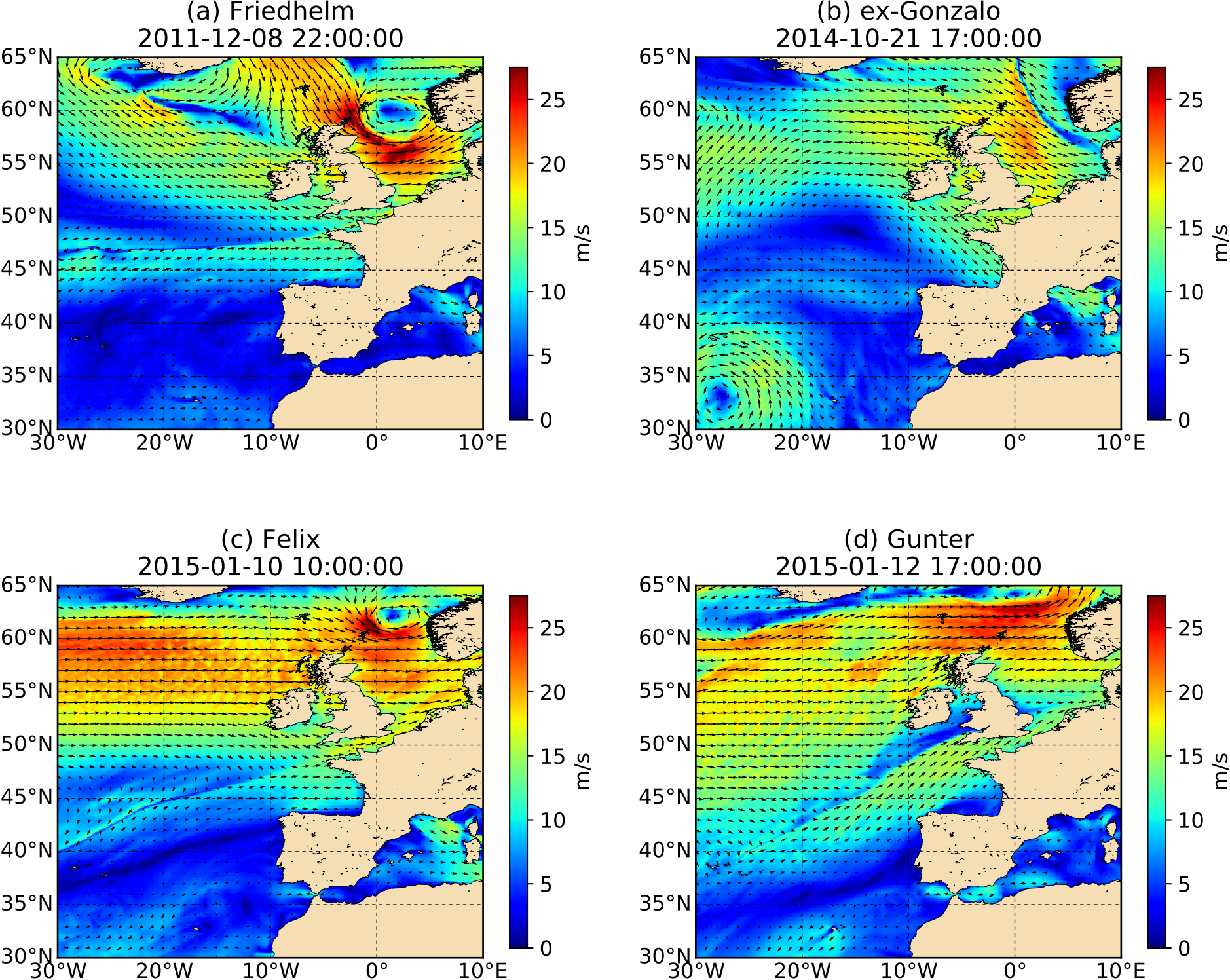
(a) Friedhelm
2011-12-08 22:00:00
(b) ex-Gonzalo
2014-10-21 17:00:00
(c) Felix
2015-01-10 10:00:00
(d) Gunter
2015-01-12 17:00:00
65°N
60°N
55°N
50°N
45°N
40°N
35°N
30°N
30°W
20°W
10°W
0°
10°E
0
5
10
15
20
25
m/s

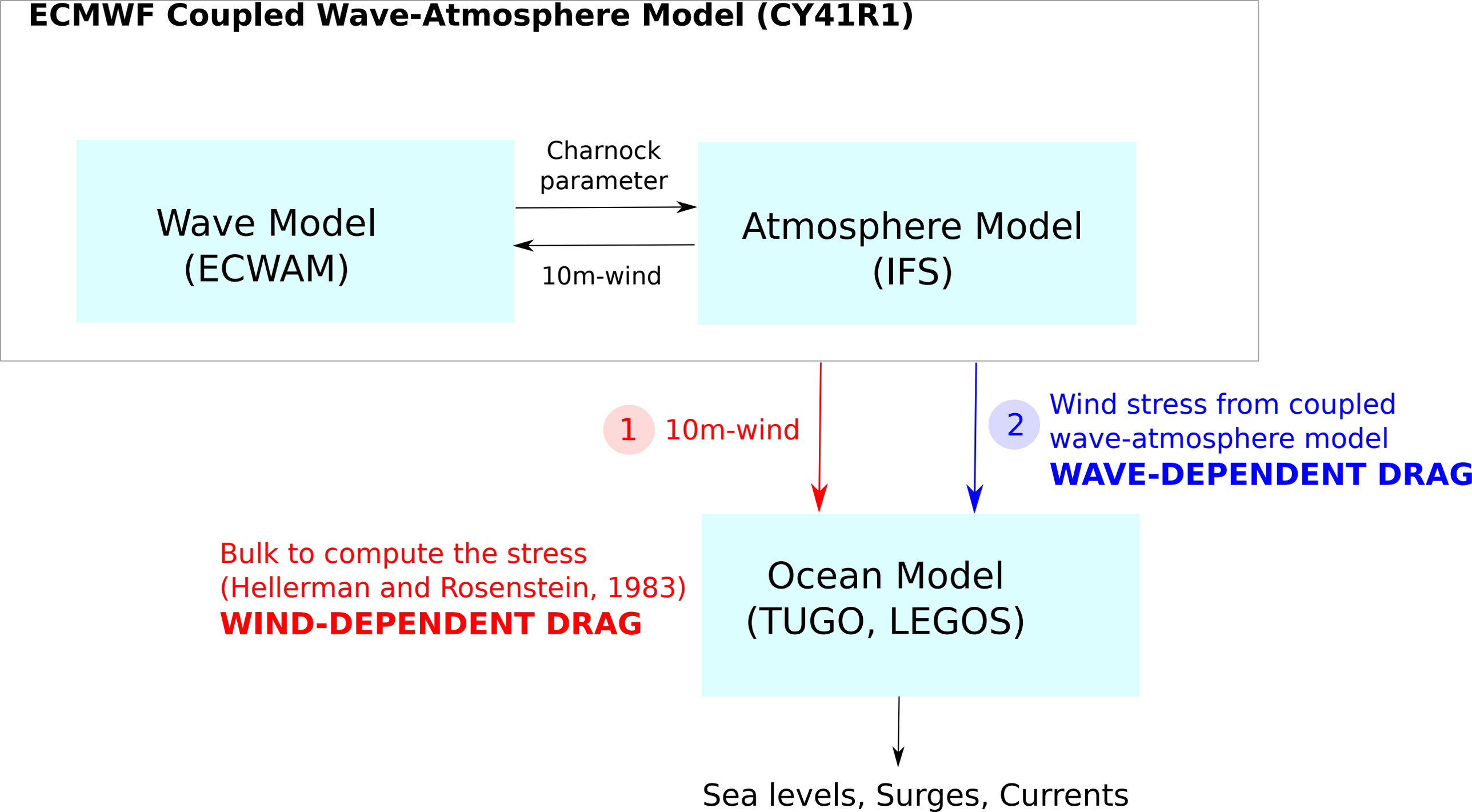
ECMWF Coupled Wave-Atmosphere Model (CY41R1)
Wave Model
(ECWAM)
Charnock
parameter
10m-wind
Atmosphere Model
(IFS)
1
10m-wind
2
Wind stress from coupled
wave-atmosphere model
WAVE-DEPENDENT DRAG
Bulk to compute the stress
(Hellerman and Rosenstein, 1983)
WIND-DEPENDENT DRAG
Ocean Model
(TUGO, LEGOS)
Sea levels, Surges, Currents

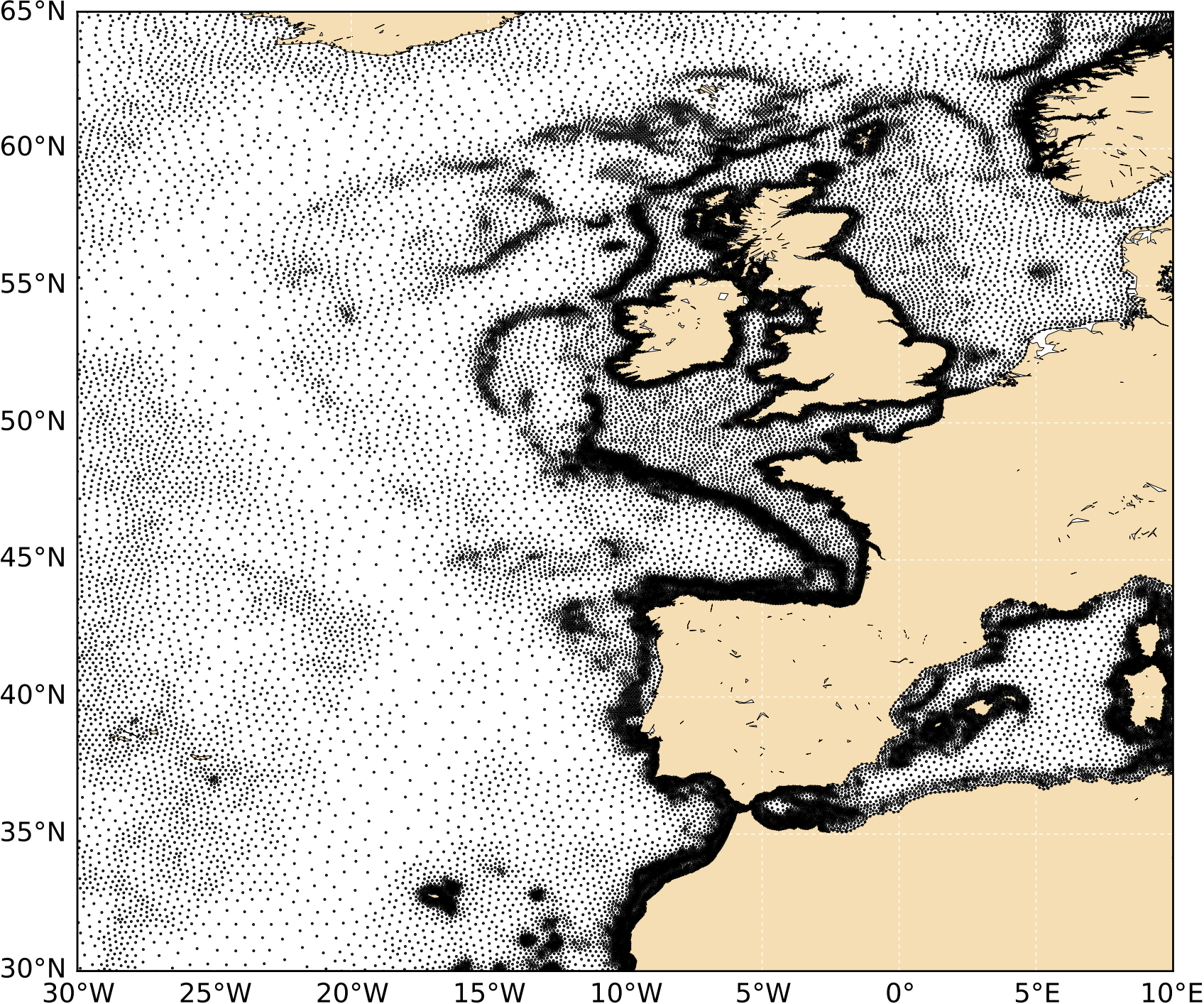
65°N
60°N
55°N
50°N
45°N
40°N
35°N
30°N
30°W
25°W
20°W
15°W
10°W
5°W
0°
5°E
10°E

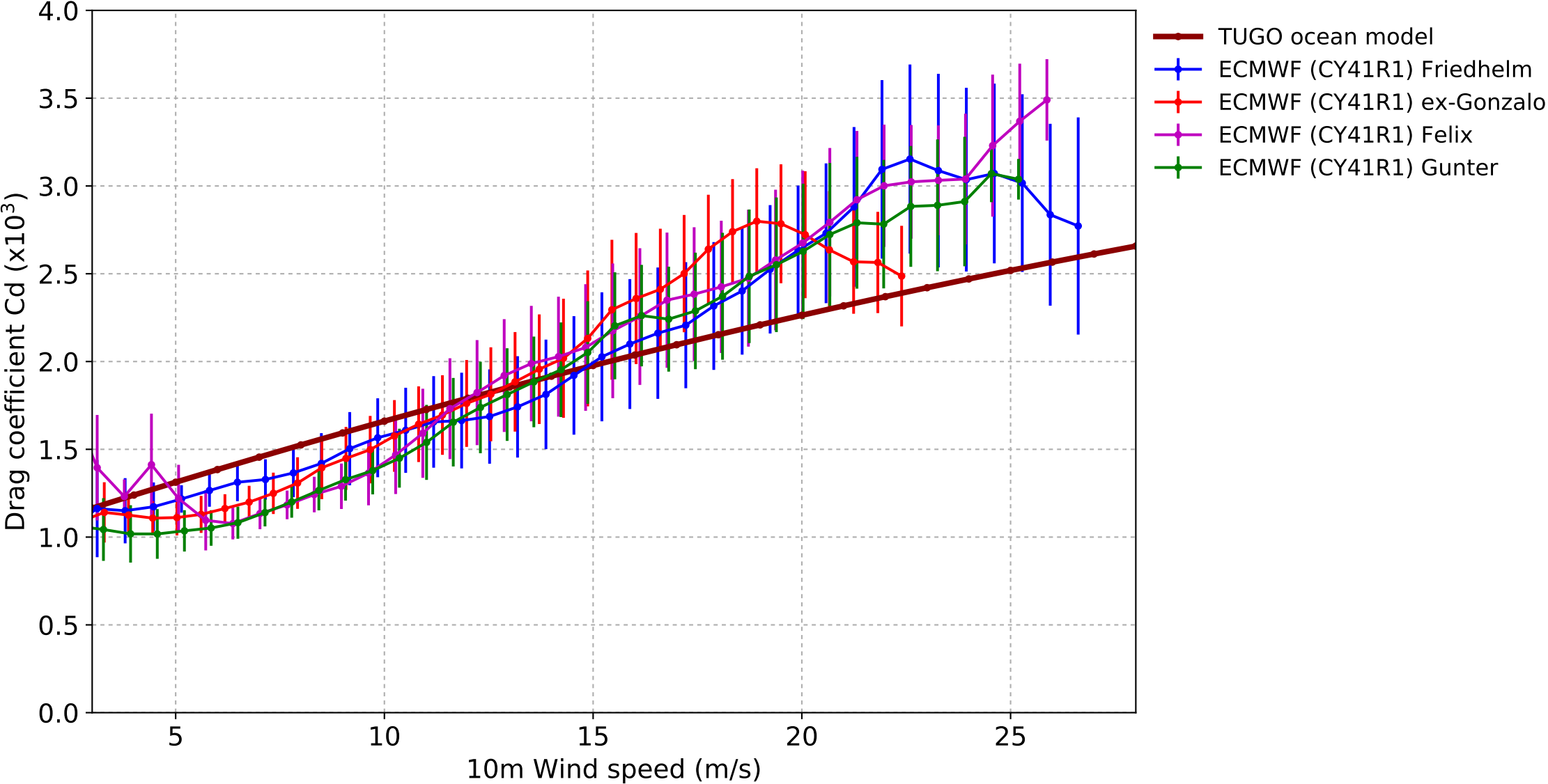
TUGO ocean model
ECMWF (CY41R1) Friedhelm
ECMWF (CY41R1) ex-Gonzalo
ECMWF (CY41R1) Felix
ECMWF (CY41R1) Gunter
Drag coefficient Cd (x10^3)
10m Wind speed (m/s)
0.0
0.5
1.0
1.5
2.0
2.5
3.0
3.5
4.0
5
10
15
20
25

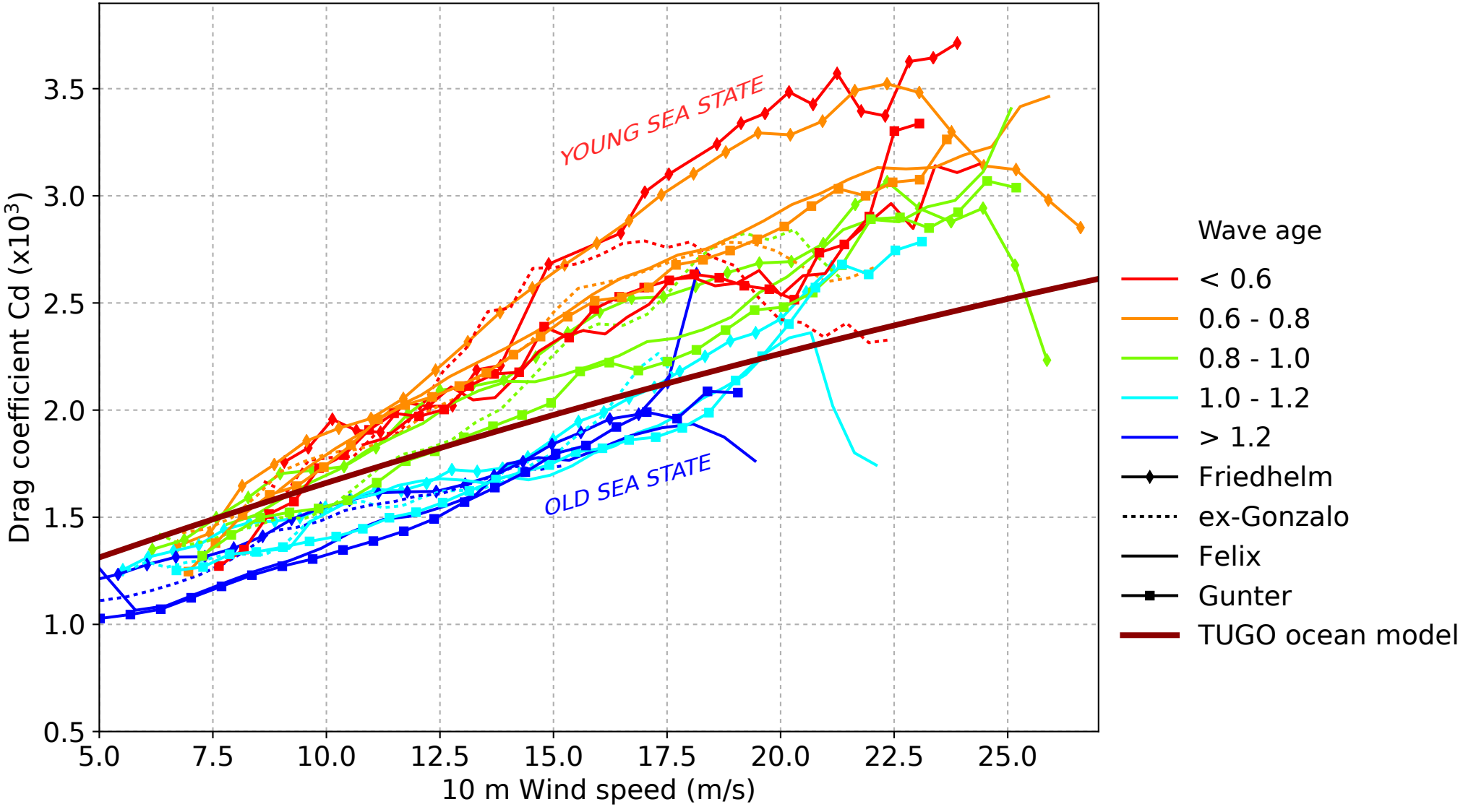
YOUNG SEA STATE
OLD SEA STATE
Drag coefficient Cd (x10^3)
3.5
3.0
2.5
2.0
1.5
1.0
0.5
5.0
7.5
10.0
12.5
15.0
17.5
20.0
22.5
25.0
10 m Wind speed (m/s)
Wave age
< 0.6
0.6 - 0.8
0.8 - 1.0
1.0 - 1.2
> 1.2
Friedhelm
ex-Gonzalo
Felix
Gunter
TUGO ocean model

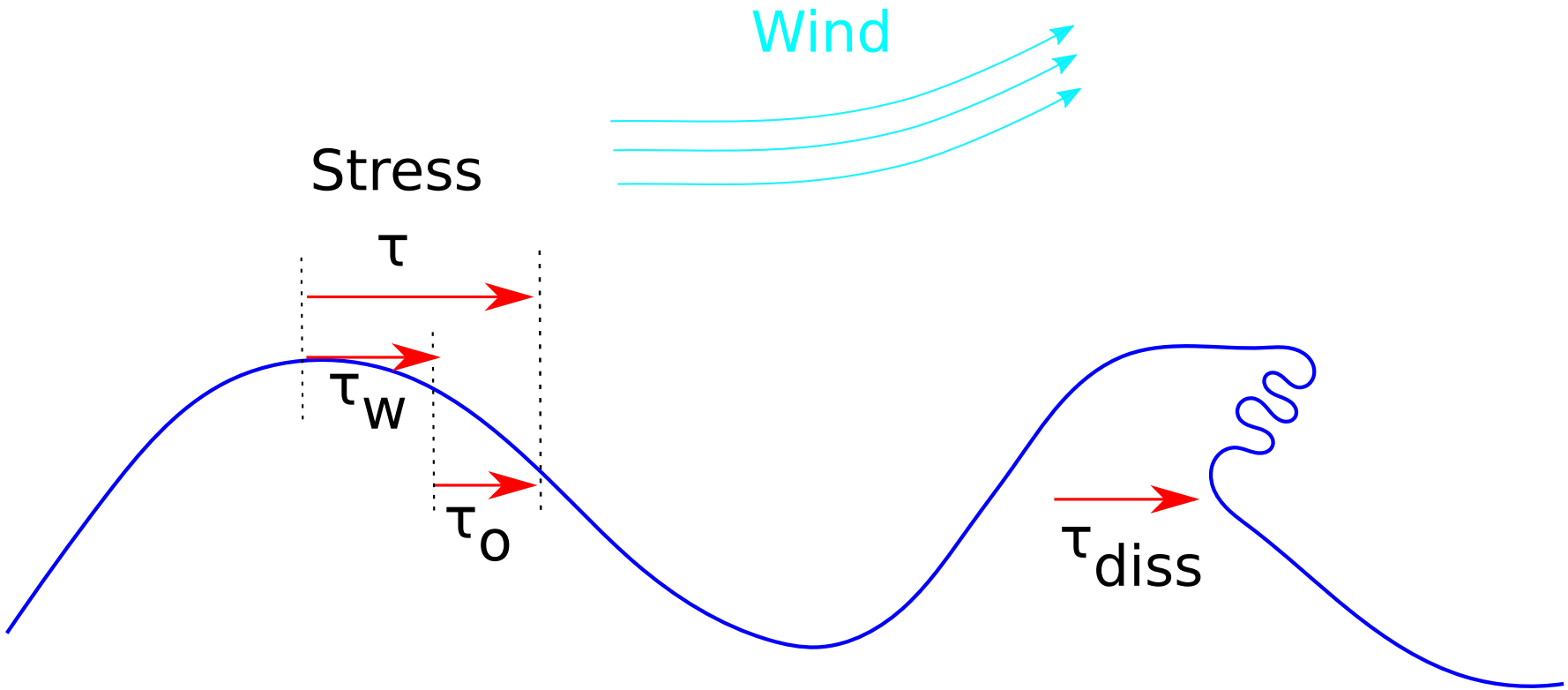
Wind
Stress
τ
τw
τo
τdiss

(a)

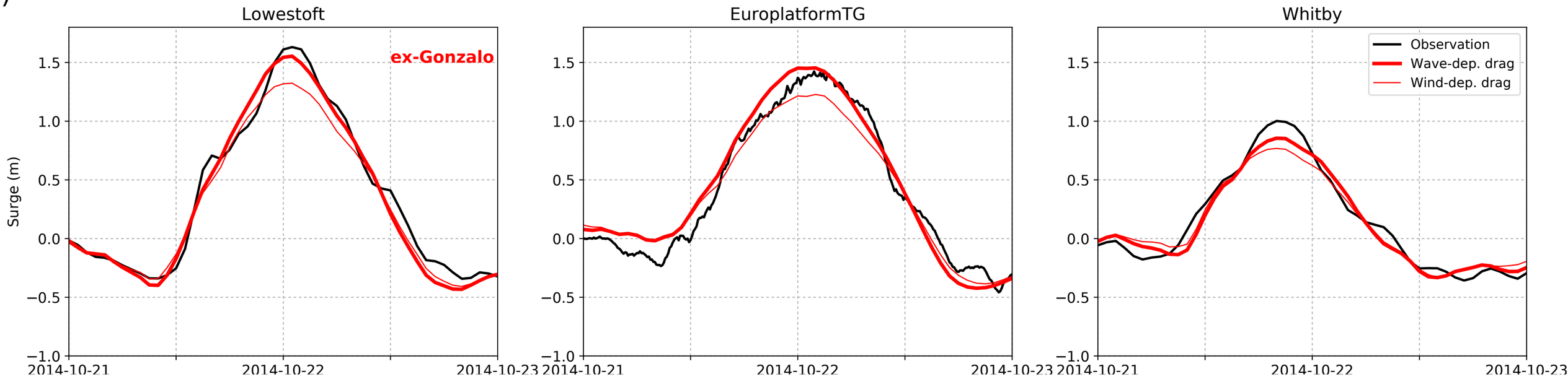
Lowestoft
EuroplatformTG
Whitby
ex-Gonzalo
Observation
Wave-dep. drag
Wind-dep. drag
Surge (m)
1.5
1.0
0.5
0.0
−0.5
−1.0
2014-10-21
2014-10-22
2014-10-23

(b)

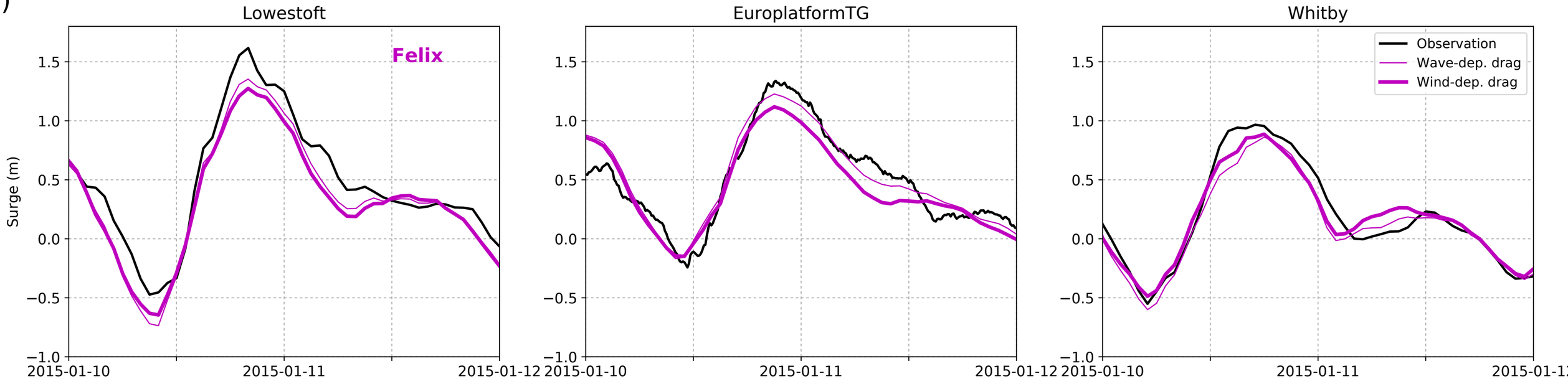
Lowestoft
EuroplatformTG
Whitby
Felix
Observation
Wave-dep. drag
Wind-dep. drag
Surge (m)
1.5
1.0
0.5
0.0
−0.5
−1.0
2015-01-10
2015-01-11
2015-01-12

(c)

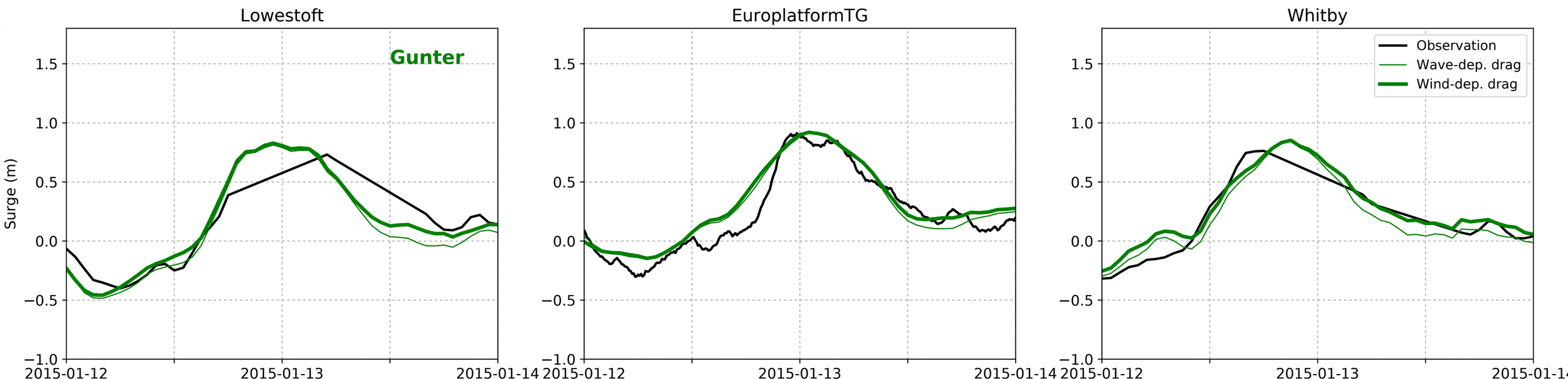
Lowestoft
EuroplatformTG
Whitby
Gunter
Observation
Wave-dep. drag
Wind-dep. drag
Surge (m)
1.5
1.0
0.5
0.0
−0.5
−1.0
2015-01-12
2015-01-13
2015-01-14

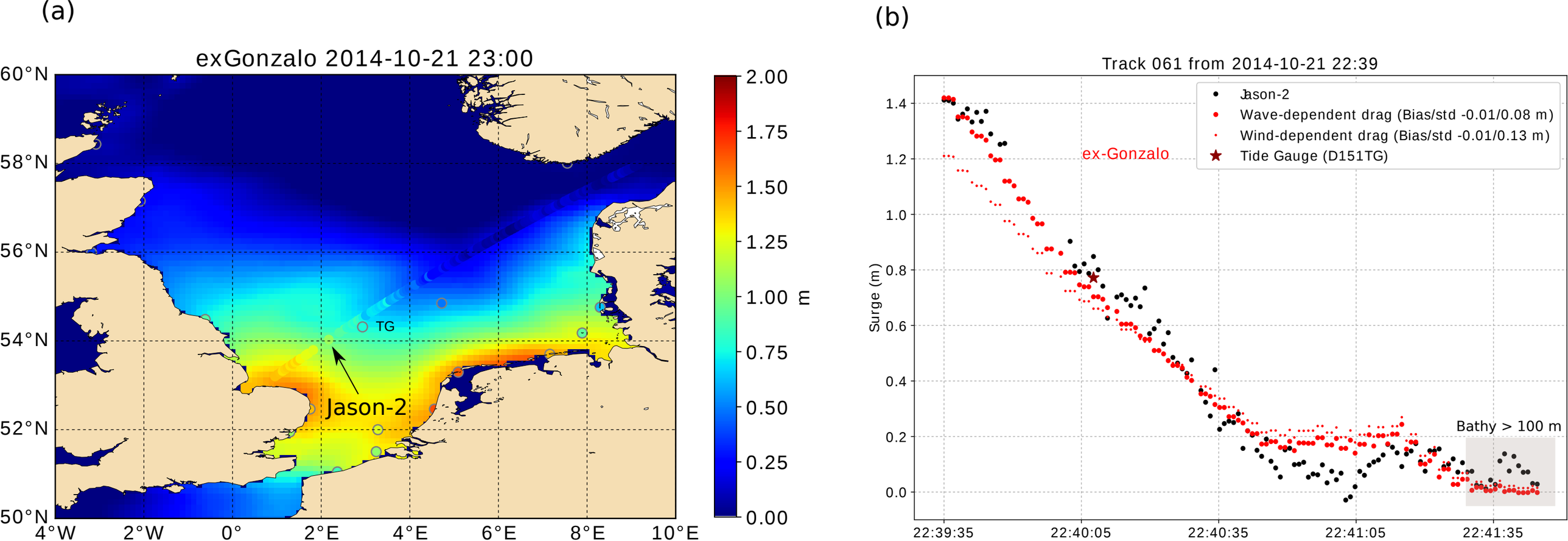
(a)
exGonzalo 2014-10-21 23:00
60°N
58°N
56°N
54°N
52°N
50°N
4°W
2°W
0°
2°E
4°E
6°E
8°E
10°E
TG
Jason-2
2.00
1.75
1.50
1.25
1.00
0.75
0.50
0.25
0.00
m
(b)
Track 061 from 2014-10-21 22:39
Jason-2
Wave-dependent drag (Bias/std -0.01/0.08 m)
Wind-dependent drag (Bias/std -0.01/0.13 m)
Tide Gauge (D151TG)
ex-Gonzalo
Surge (m)
1.4
1.2
1.0
0.8
0.6
0.4
0.2
0.0
Bathy > 100 m
22:39:35
22:40:05
22:40:35
22:41:05
22:41:35

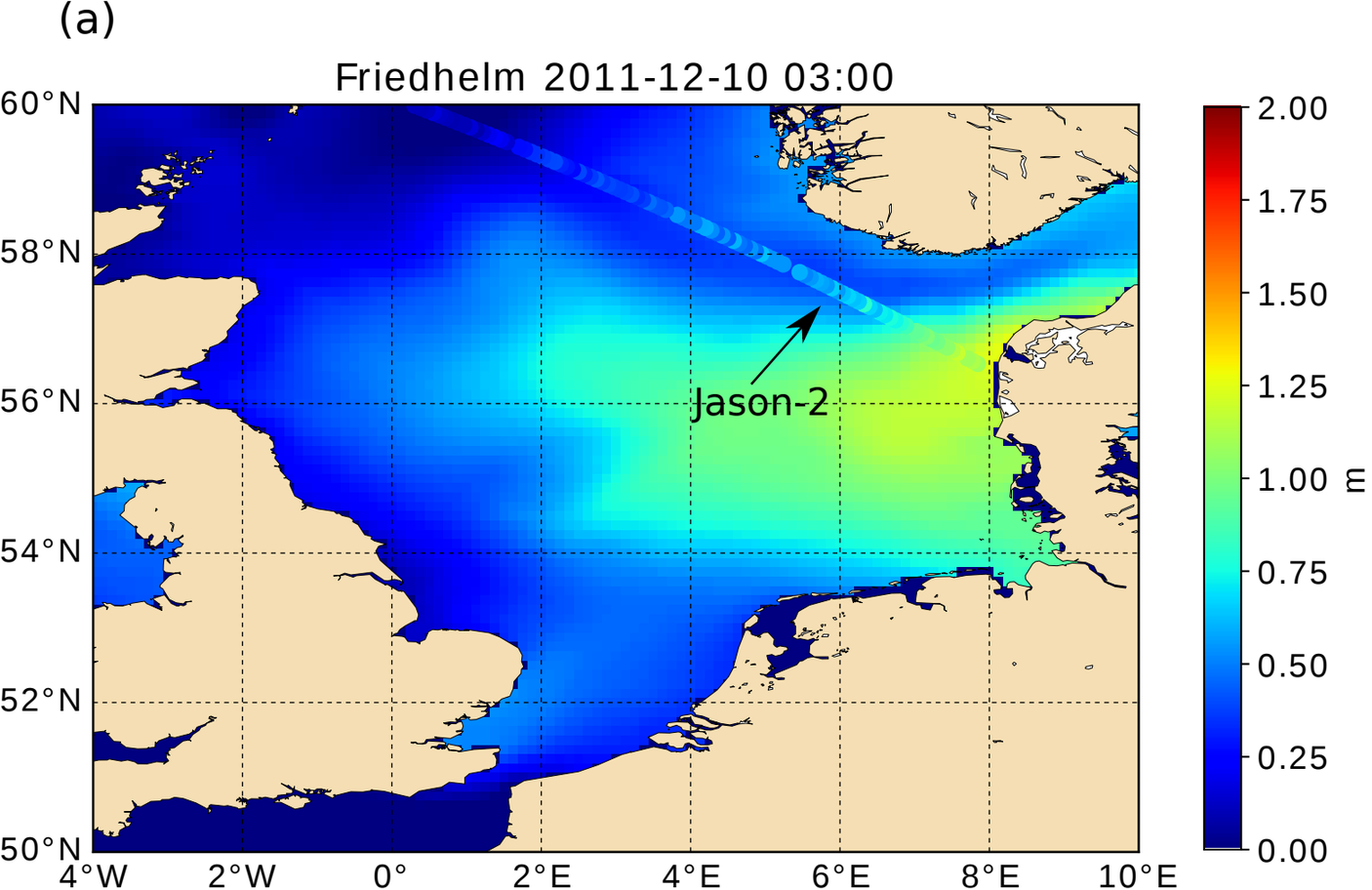
(a)
Friedhelm 2011-12-10 03:00
60°N
58°N
56°N
54°N
52°N
50°N
4°W
2°W
0°
2°E
4°E
6°E
8°E
10°E
Jason-2
2.00
1.75
1.50
1.25
1.00
0.75
0.50
0.25
0.00
m

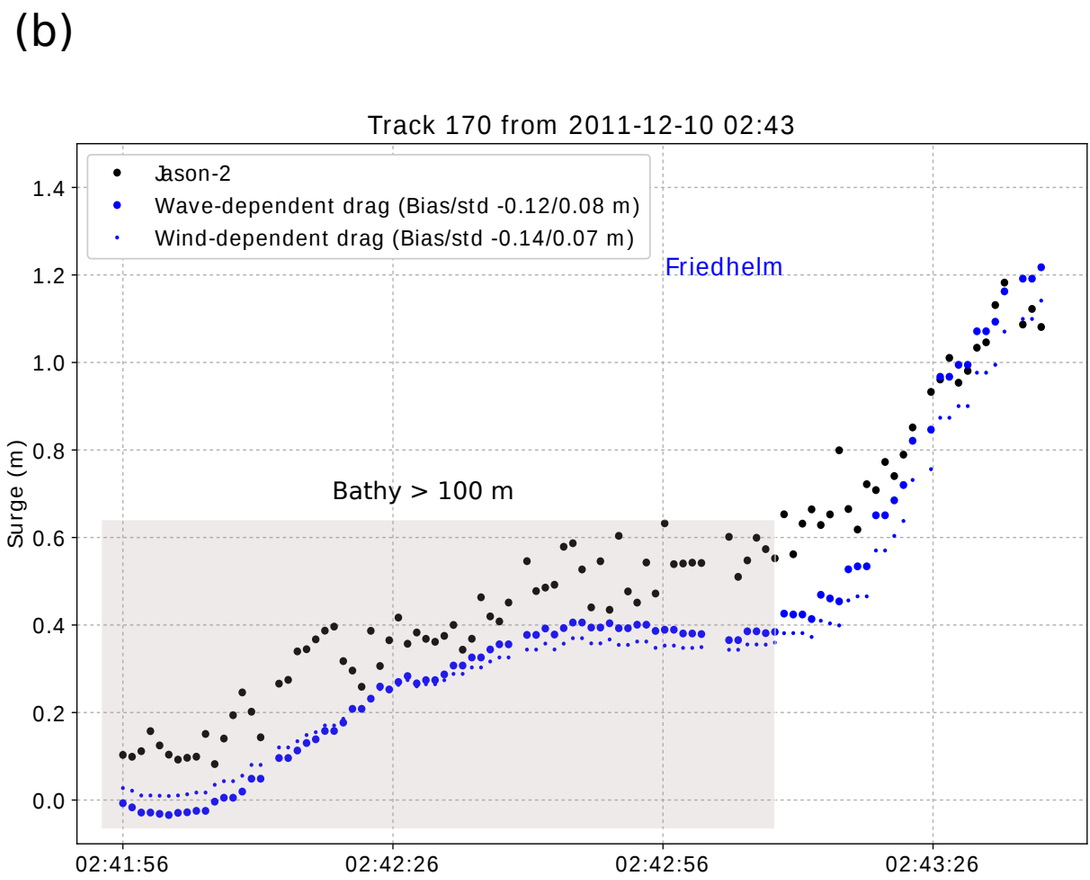
(b)
Track 170 from 2011-12-10 02:43
Jason-2
Wave-dependent drag (Bias/std -0.12/0.08 m)
Wind-dependent drag (Bias/std -0.14/0.07 m)
Friedhelm
Bathy > 100 m
Surge (m)
1.4
1.2
1.0
0.8
0.6
0.4
0.2
0.0
02:41:56
02:42:26
02:42:56
02:43:26

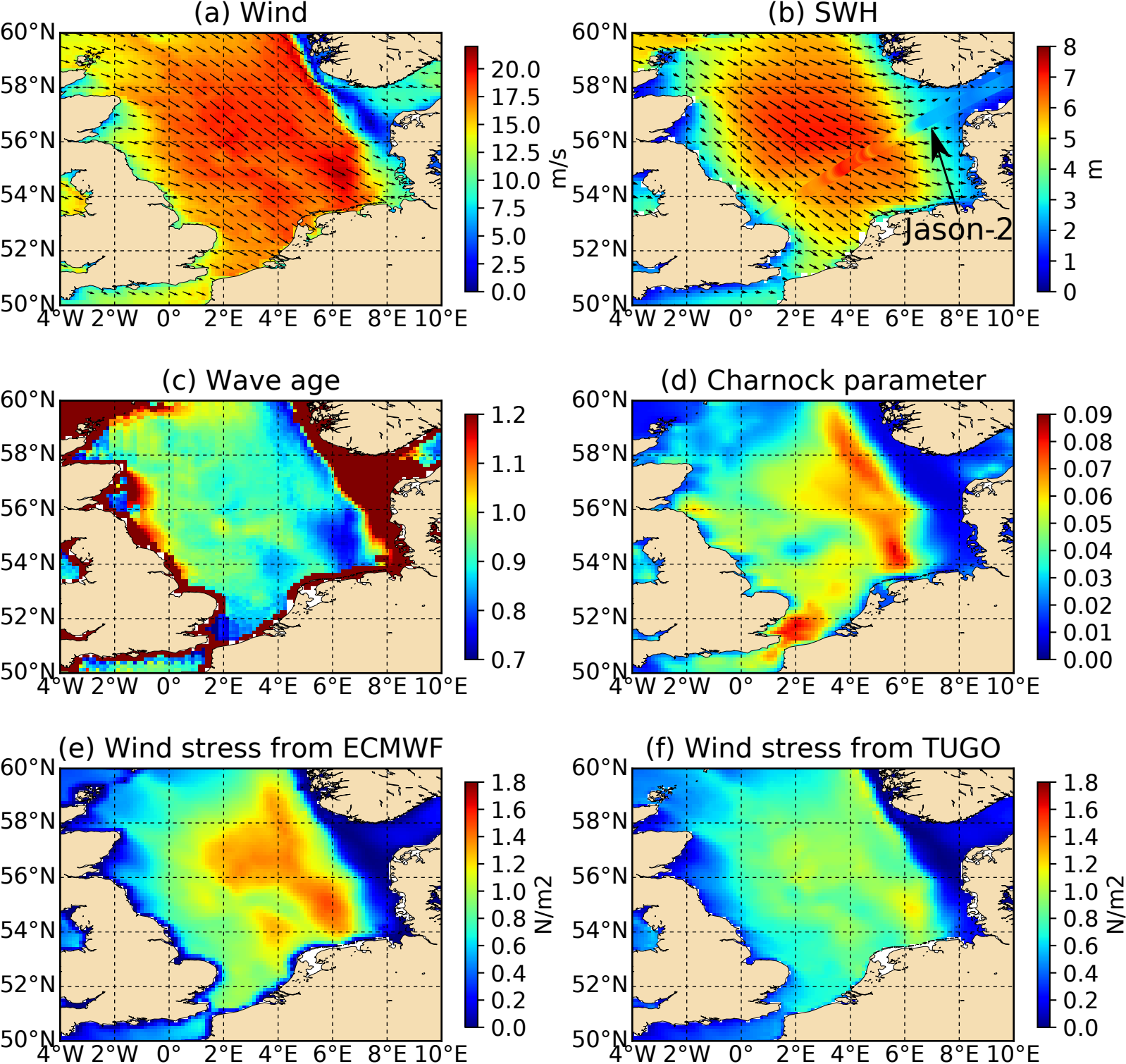
(a) Wind
(b) SWH
(c) Wave age
(d) Charnock parameter
(e) Wind stress from ECMWF
(f) Wind stress from TUGO
Jason-2
m/s
m
N/m2
60°N
58°N
56°N
54°N
52°N
50°N
4°W 2°W 0° 2°E 4°E 6°E 8°E 10°E
20.0 17.5 15.0 12.5 10.0 7.5 5.0 2.5 0.0
8 7 6 5 4 3 2 1 0
1.2 1.1 1.0 0.9 0.8 0.7
0.09 0.08 0.07 0.06 0.05 0.04 0.03 0.02 0.01 0.00
1.8 1.6 1.4 1.2 1.0 0.8 0.6 0.4 0.2 0.0

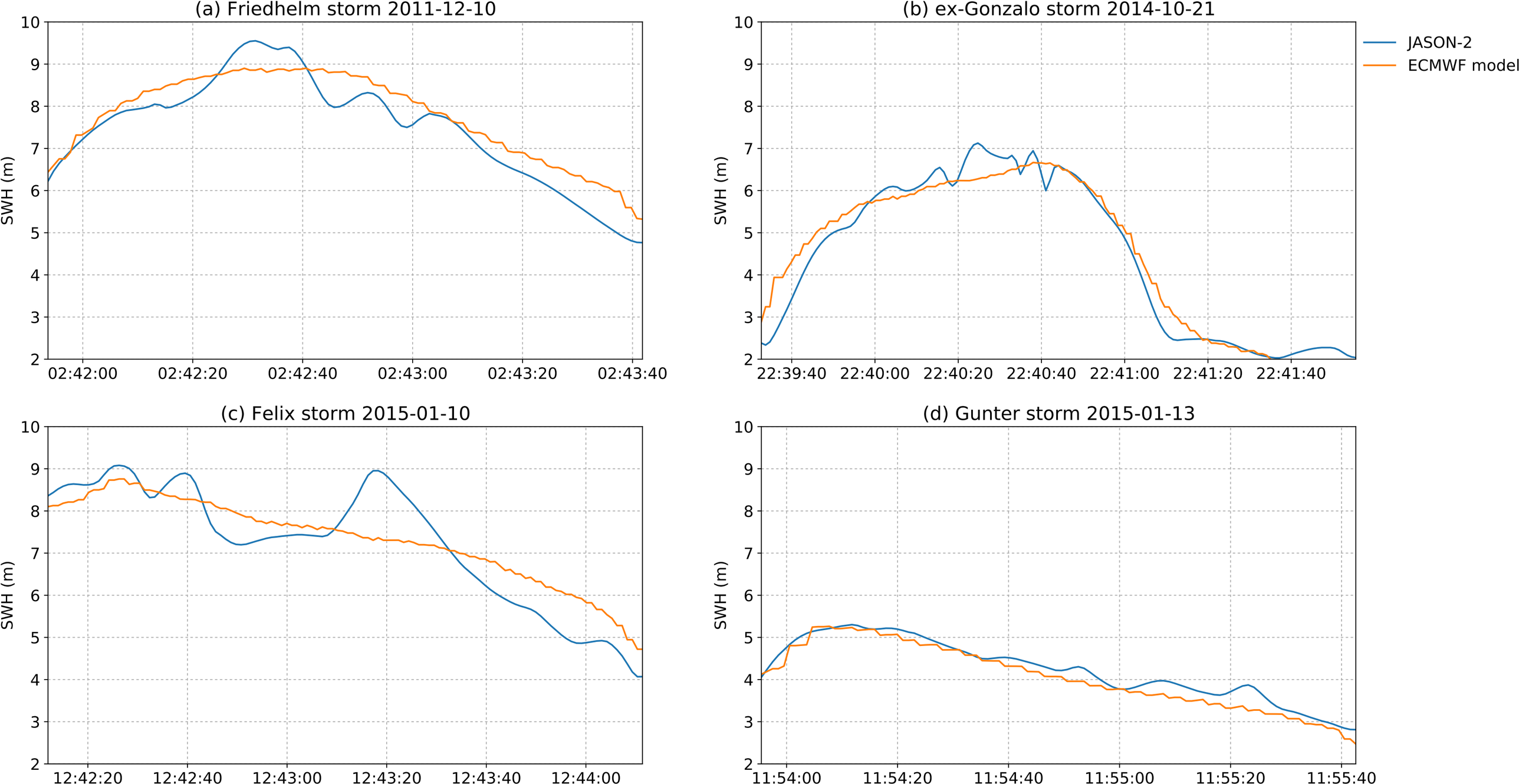
(a) Friedhelm storm 2011-12-10
(b) ex-Gonzalo storm 2014-10-21
(c) Felix storm 2015-01-10
(d) Gunter storm 2015-01-13
SWH (m)
JASON-2
ECMWF model
02:42:00
02:42:20
02:42:40
02:43:00
02:43:20
02:43:40
22:39:40
22:40:00
22:40:20
22:40:40
22:41:00
22:41:20
22:41:40
12:42:20
12:42:40
12:43:00
12:43:20
12:43:40
12:44:00
11:54:00
11:54:20
11:54:40
11:55:00
11:55:20
11:55:40

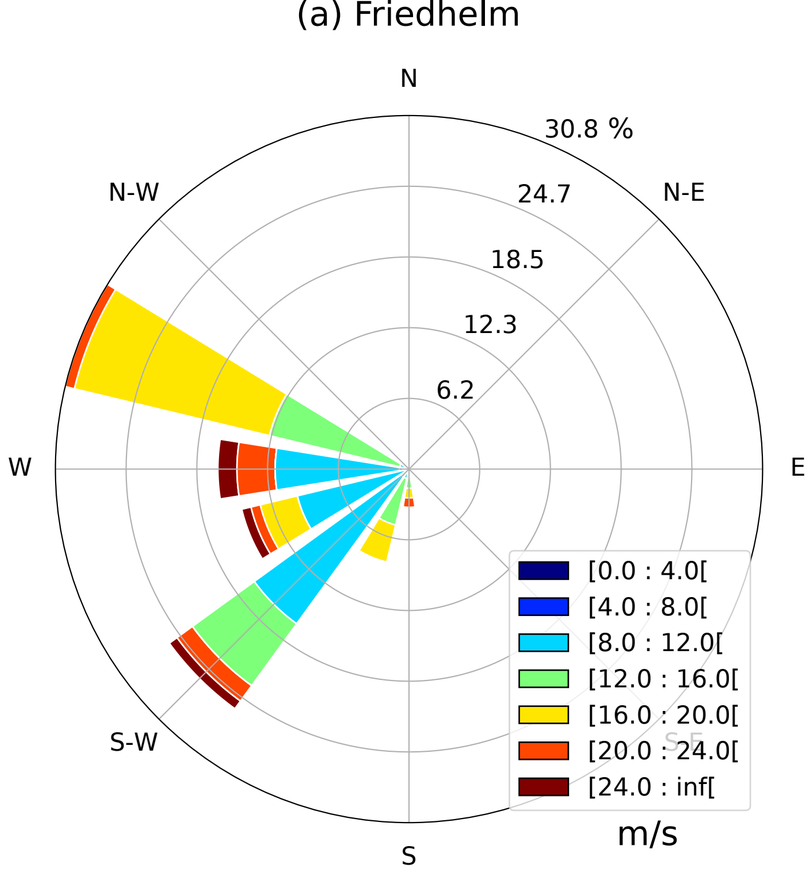
(a) Friedhelm
N
N-E
E
S-E
S
S-W
W
N-W
30.8 %
24.7
18.5
12.3
6.2
[0.0 : 4.0[
[4.0 : 8.0[
[8.0 : 12.0[
[12.0 : 16.0[
[16.0 : 20.0[
[20.0 : 24.0[
[24.0 : inf[
m/s

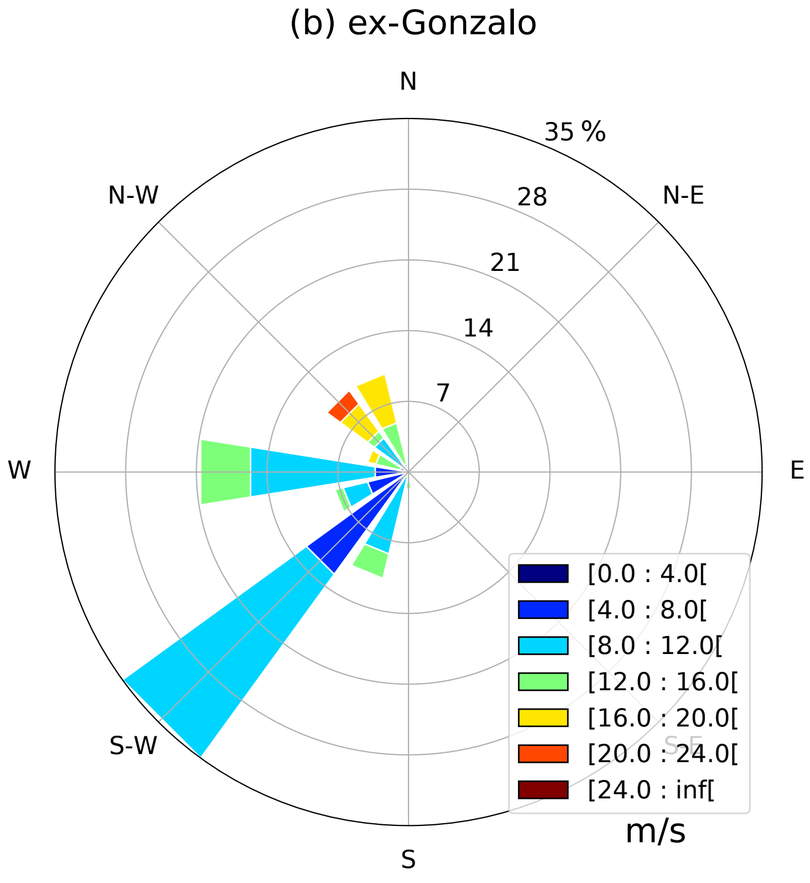
(b) ex-Gonzalo
N
N-E
E
S-E
S
S-W
W
N-W
35 %
28
21
14
7
[0.0 : 4.0[
[4.0 : 8.0[
[8.0 : 12.0[
[12.0 : 16.0[
[16.0 : 20.0[
[20.0 : 24.0[
[24.0 : inf[
m/s

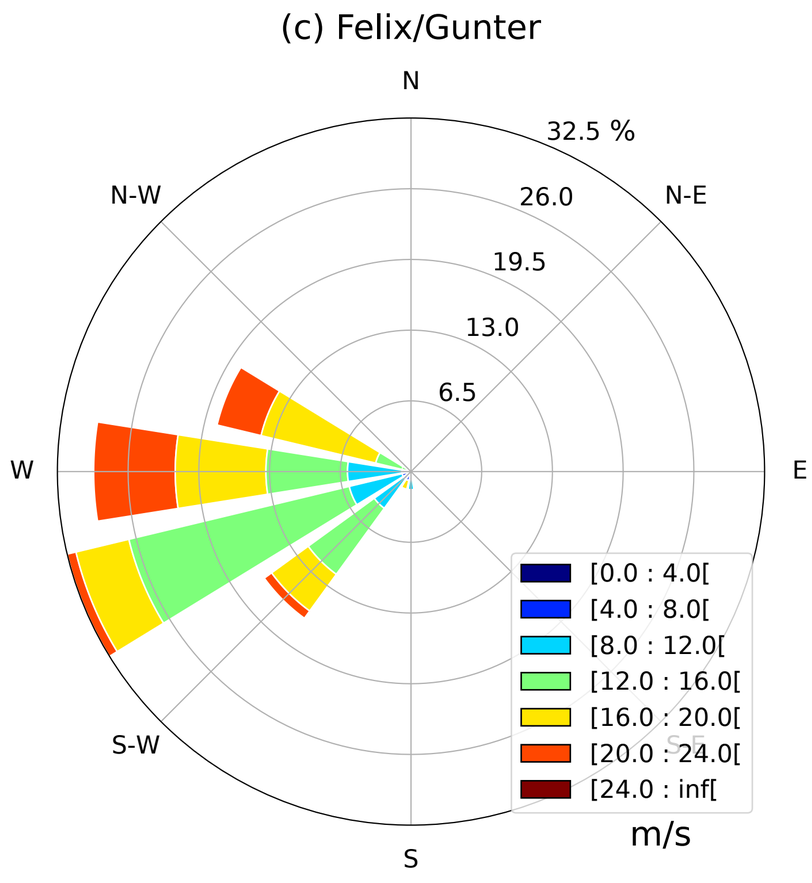
(c) Felix/Gunter
N
N-E
E
S-E
S
S-W
W
N-W
32.5 %
26.0
19.5
13.0
6.5
[0.0 : 4.0[
[4.0 : 8.0[
[8.0 : 12.0[
[12.0 : 16.0[
[16.0 : 20.0[
[20.0 : 24.0[
[24.0 : inf[
m/s

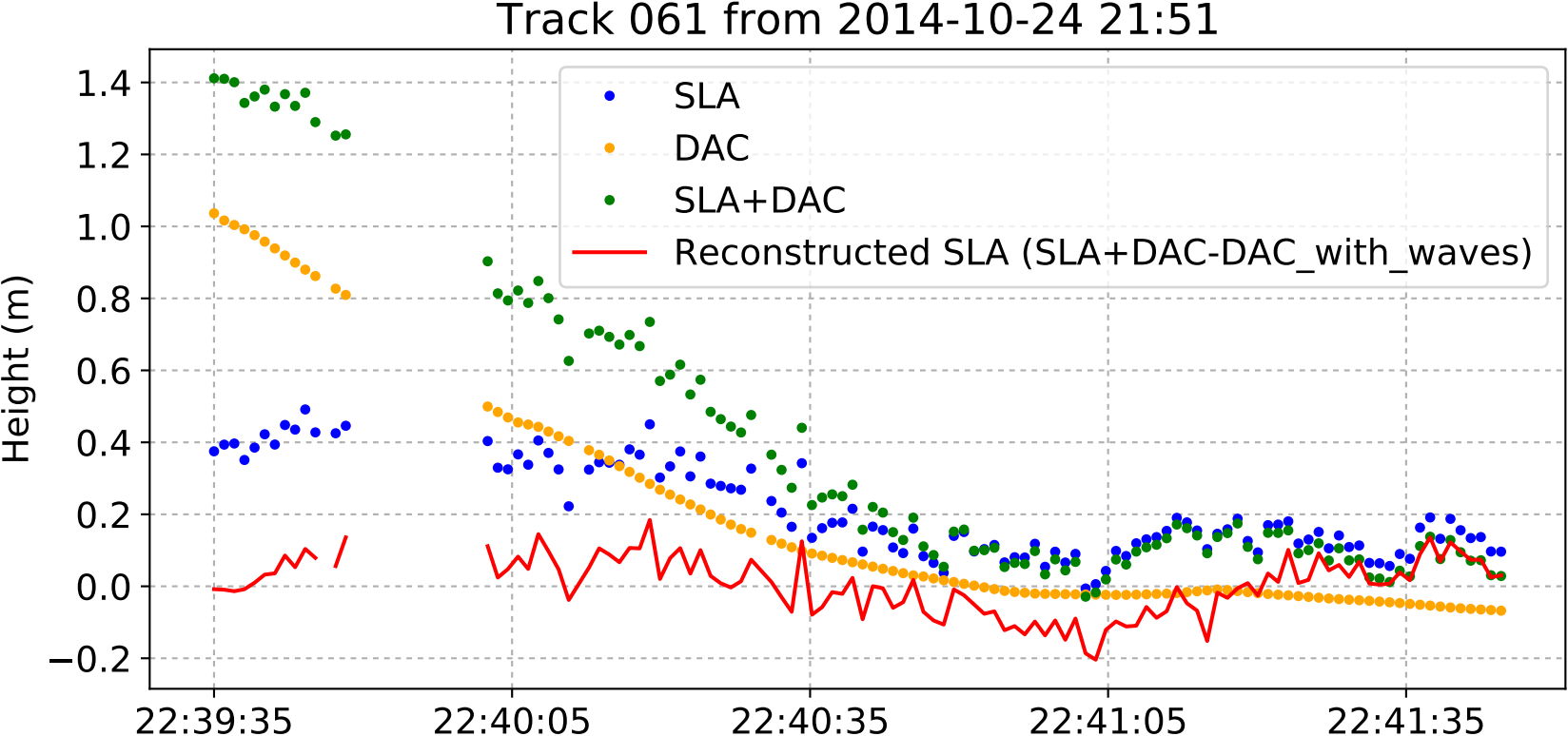
Track 061 from 2014-10-24 21:51
Height (m)
1.4
1.2
1.0
0.8
0.6
0.4
0.2
0.0
−0.2
22:39:35
22:40:05
22:40:35
22:41:05
22:41:35
SLA
DAC
SLA+DAC
Reconstructed SLA (SLA+DAC-DAC_with_waves)